Journal club

Grover's algorithm in a four-qubit silicon processor above the fault-tolerant threshold

I. Thorvaldson,[1,2,*] D. Poulos,[1,*] C. M. Moehle,[1,*] S. H. Misha,[1] H. Edlbauer,[1] J. Reiner,[1]
H. Geng,[1] B. Voisin,[1] M. T. Jones,[1] M. B. Donnelly,[1,2] L. F. Peña,[1] C. D. Hill,[1,2] C. R. Myers,[1,2]
J. G. Keizer,[1,2] Y. Chung,[1] S. K. Gorman,[1,2,†] L. Kranz,[1,2,†] and M. Y. Simmons[1,2,‡]
[1] *Silicon Quantum Computing Pty Ltd., UNSW Sydney, Australia*
[2] *Centre of Excellence for Quantum Computation and Communication Technology, UNSW Sydney, Australia*
(Dated: April 16, 2024)

5	3			7				
6			1	9	5			
	9	8					6	
8				6				3
4			8		3			1
7				2				6
	6					2	8	
			4	1	9			5
				8			7	9

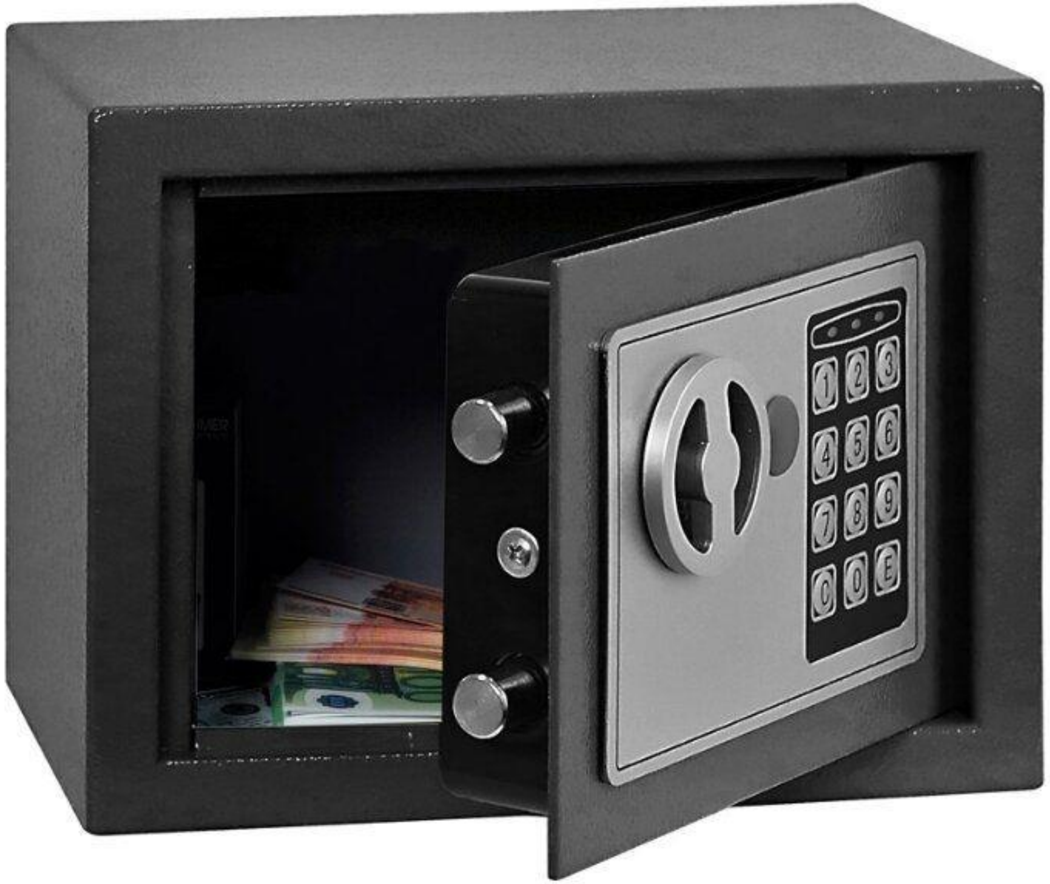

O(N) complexity

Problem: $f\colon \{0,1,\ldots,N-1\} \to \{0,1\}$ $f(x)$ = 1 only for w-index

1. ***Initialisation*** $|s\rangle = \frac{1}{\sqrt{N}} \sum_{x=0}^{N-1} |x\rangle.$

2. ***Oracle*** operator

$$\begin{cases} U_\omega|x\rangle = -|x\rangle & \text{for } x = \omega, \text{ that is, } f(x) = 1, \\ U_\omega|x\rangle = |x\rangle & \text{for } x \neq \omega, \text{ that is, } f(x) = 0. \end{cases}$$

3. ***Grover diffusion*** operator

$$U_s = 2\,|s\rangle\,\langle s| - I$$

$$O(\sqrt{N})$$

To find the marked state

Unlike other quantum algorithms, which may provide exponential speedup over their classical counterparts, **Grover's algorithm** provides only a **quadratic speedup**

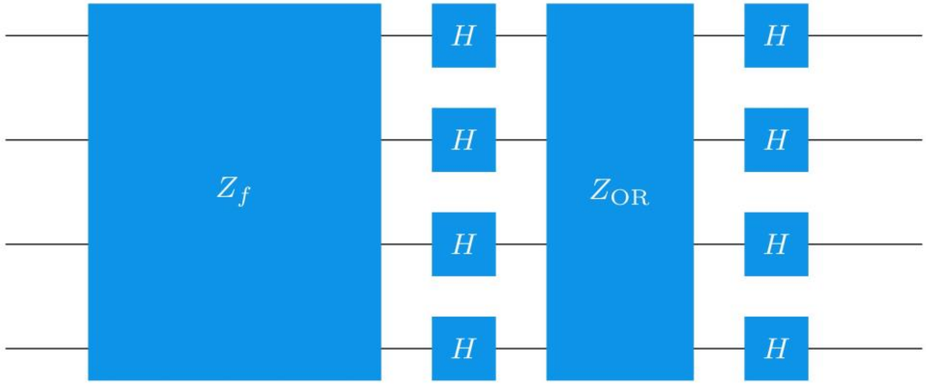

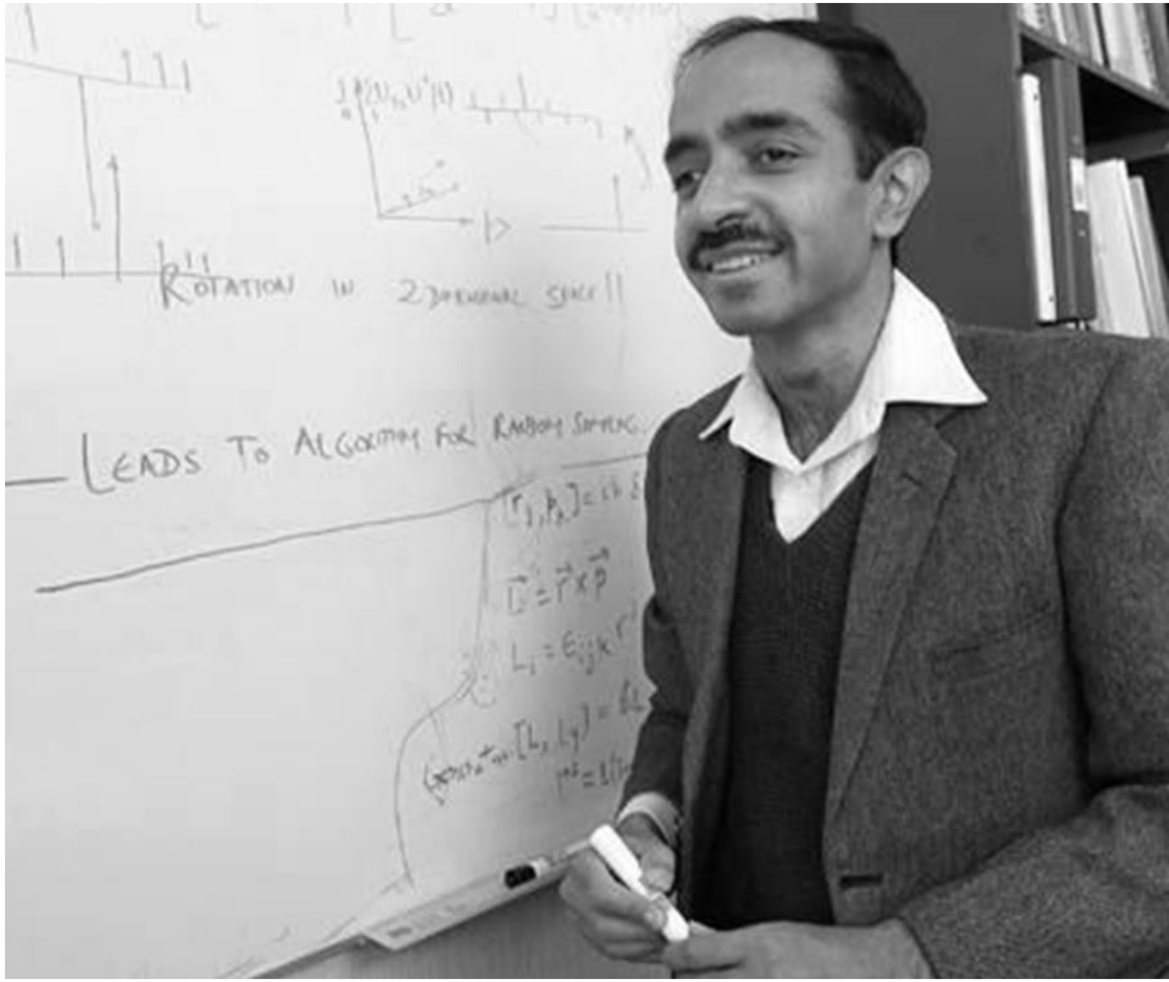

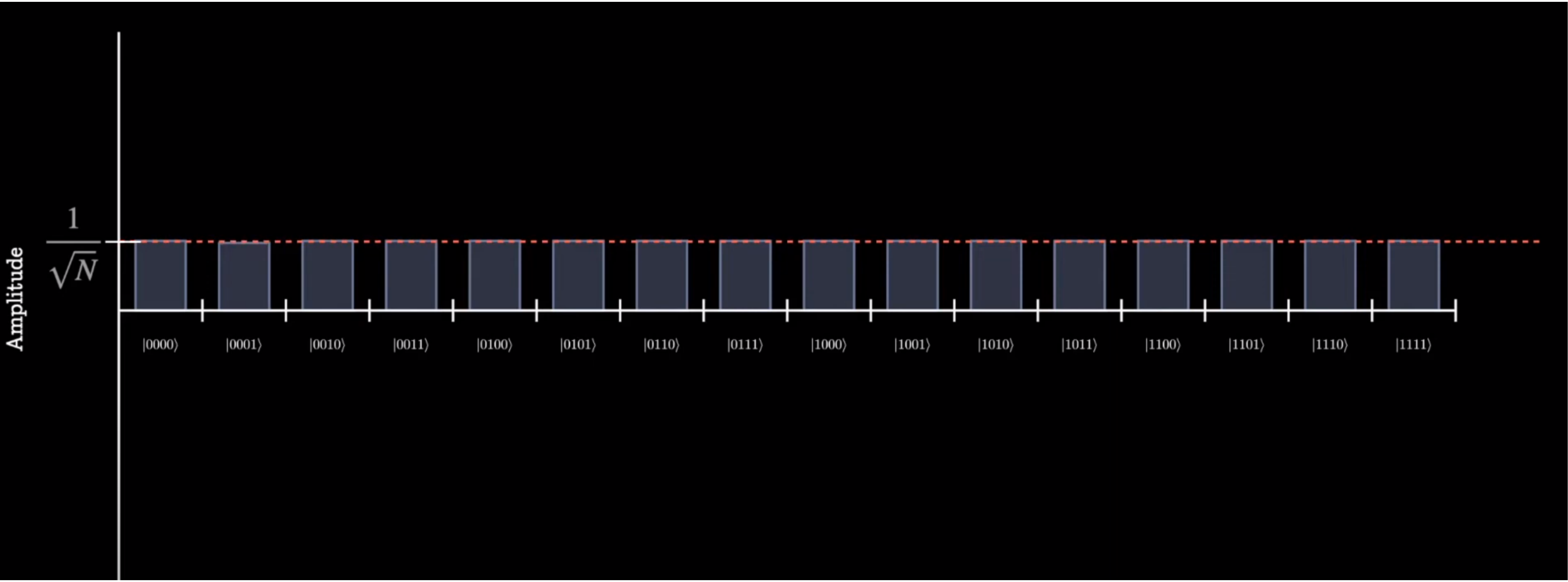
Amplitude
$\frac{1}{\sqrt{N}}$
|0000⟩
|0001⟩
|0010⟩
|0011⟩
|0100⟩
|0101⟩
|0110⟩
|0111⟩
|1000⟩
|1001⟩
|1010⟩
|1011⟩
|1100⟩
|1101⟩
|1110⟩
|1111⟩

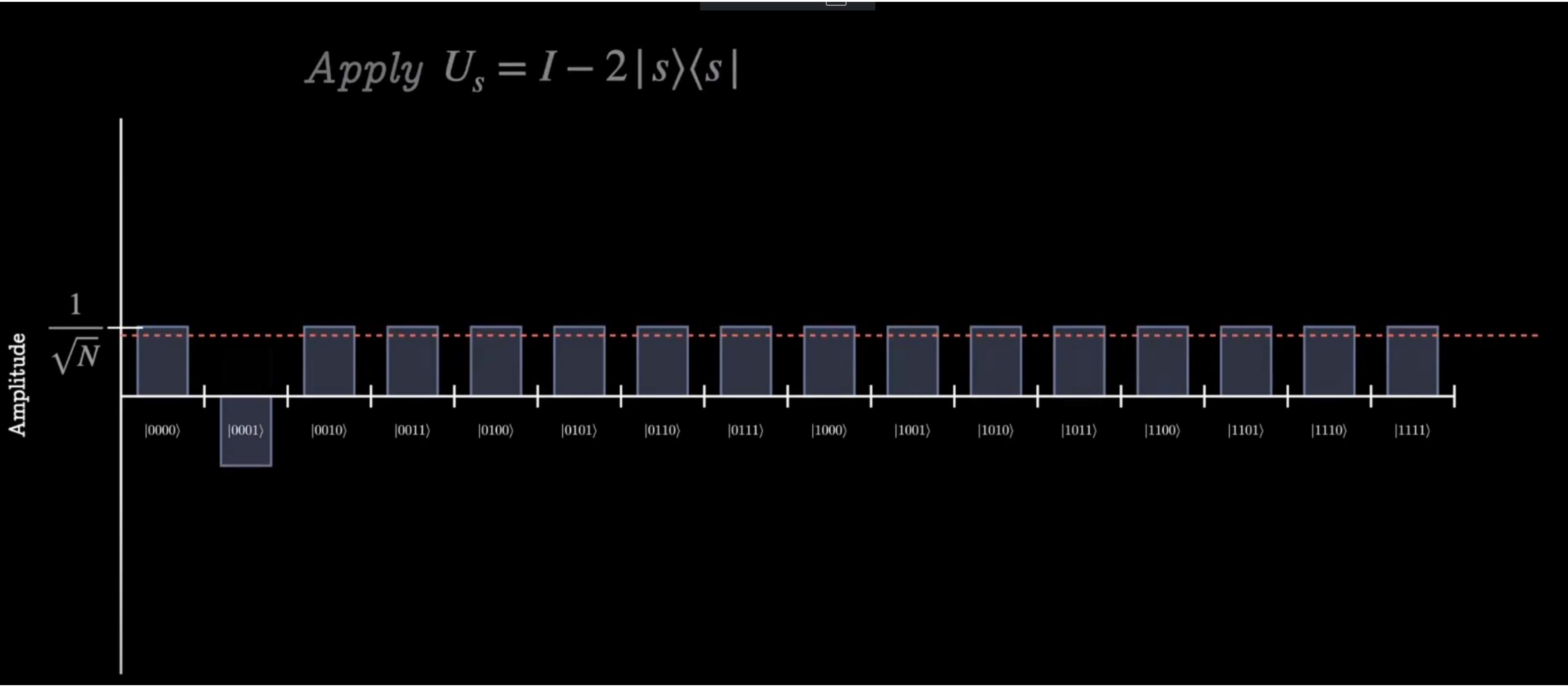

$Apply\ U_s = I - 2|s\rangle\langle s|$
Amplitude
$\frac{1}{\sqrt{N}}$
$|0000\rangle$
$|0001\rangle$
$|0010\rangle$
$|0011\rangle$
$|0100\rangle$
$|0101\rangle$
$|0110\rangle$
$|0111\rangle$
$|1000\rangle$
$|1001\rangle$
$|1010\rangle$
$|1011\rangle$
$|1100\rangle$
$|1101\rangle$
$|1110\rangle$
$|1111\rangle$

$$Apply\ U_d = 2|\phi\rangle\langle\phi| - I$$

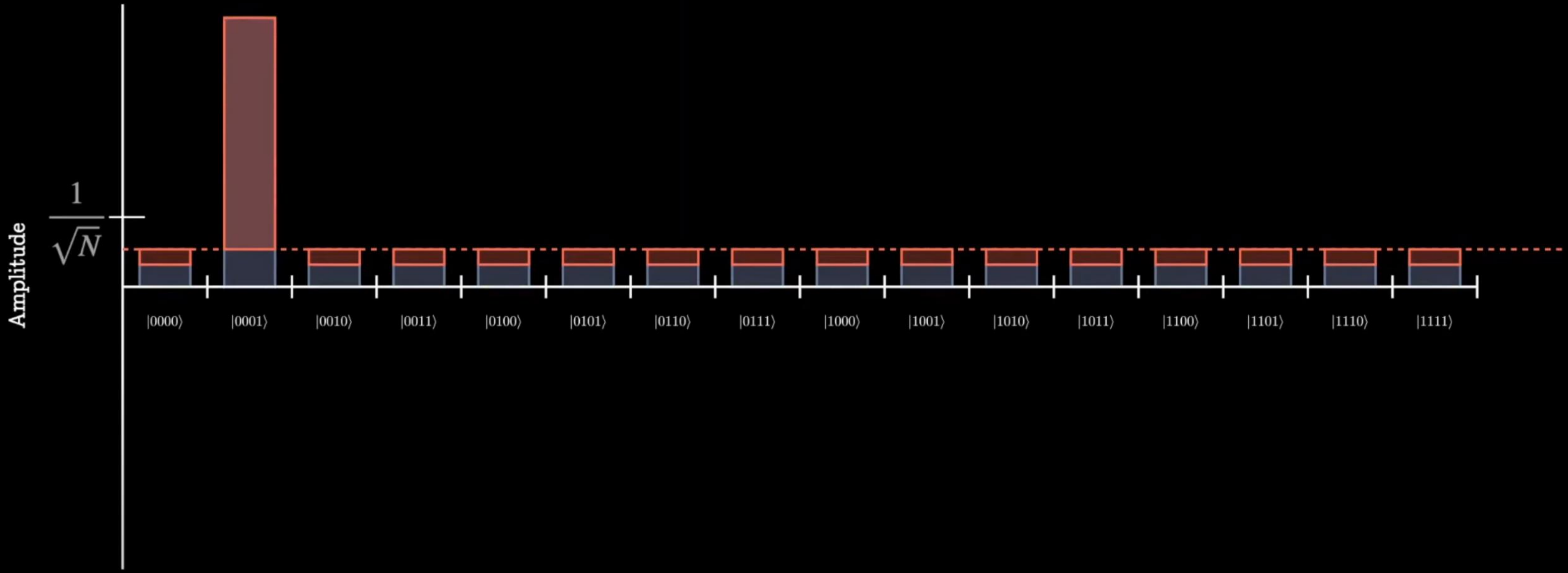

Reference	Xue [5]	Noiri [6]	Takeda [15]	Philips [16]	Hendrickx [23] Van Riggelen [24]	Madzik [8]	This work
Year	2022	2022	2022	2022	2021/2022	2022	2024
Platform	Si/SiGe	Si/SiGe	Si/SiGe	Si/SiGe	Ge/SiGe	Si:P	Si:P
Qubits	2 (electrons)	2 (electrons)	3 (electrons)	6 (electrons)	4 (holes)	3 (n-n-e)	4 (n-n-n-e)
SPAM fidelity (%)	-	74.25^a	-	-	-	98.95^a (n)	99.42 to 99.57 (n)
Rabi visibility (%)	-	-	70 to 85^b	93.5 to 98^c	60 to 75^b	-	92 to 99 (n)
Single-qubit gate fidelity (%)	99.71 to 99.74	99.84 to 99.84	99.68 to 99.77	99.77 to 99.96	99.40 to 99.88	99.46 to 99.91 (n)	99.95 to 99.98 (n)
Two-qubit gate fidelity (%)	99.65	99.51	-	-	-	99.37 (n-n)	99.32 to 99.65 (n-n)
Bell state fidelity (%)	98.1^d (w/o SPAM)	96.5 (w/o SPAM)	-	78.0 to 91.3	-	93.4 (n-n)	96.8 to 97.7 (n-n)
Three-qubit GHZ state fidelity (%)	N/A	N/A	86.6 (w/o SPAM)	52.7 to 67.2	-	92.5^e (n-n-e)	96.2 (n-n-n)
Demonstration of algorithm or QEC	Two-qubit VQE algorithm	Two-qubit DJ and Grover's algorithm	Three-qubit phase-flip QEC code	-	Three-qubit phase-flip QEC code	-	Three-qubit Grover's algorithm

State-of-the-art semiconductor spin qubit quantum processors

Universität Basel

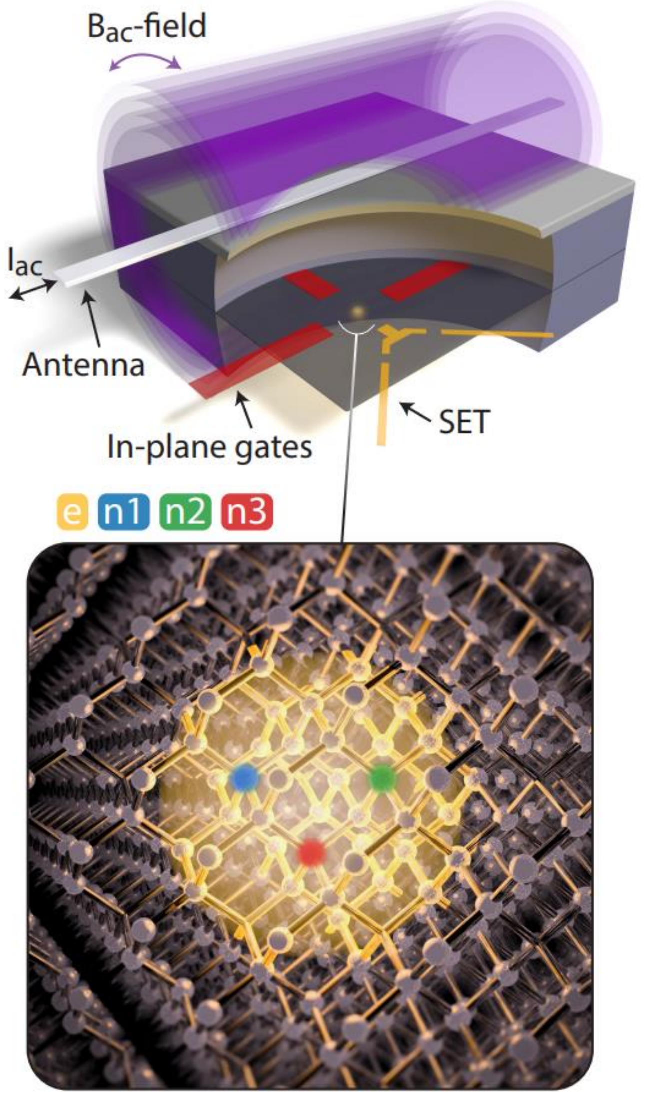

https://arxiv.org/pdf/2404.08741

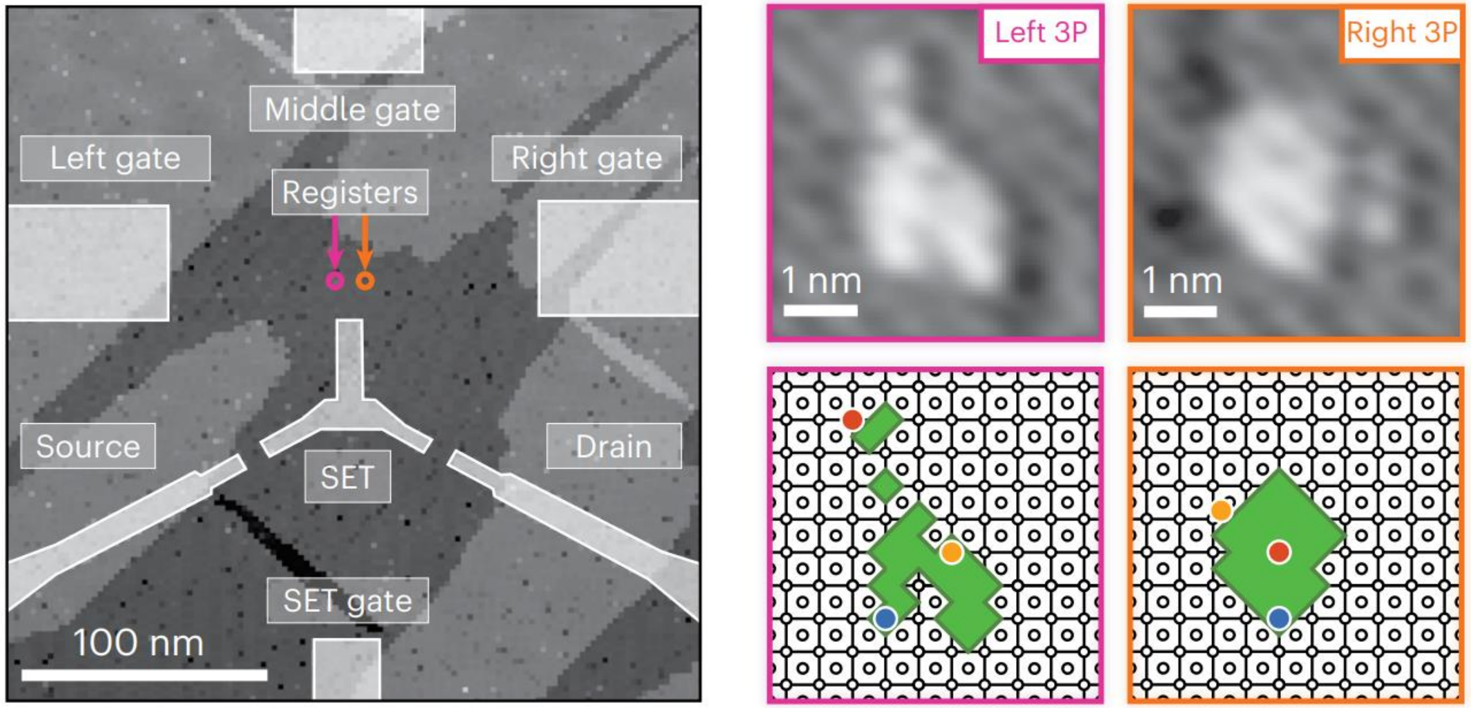

https://www.nature.com/articles/s41565-023-01596-9

Device Configuration

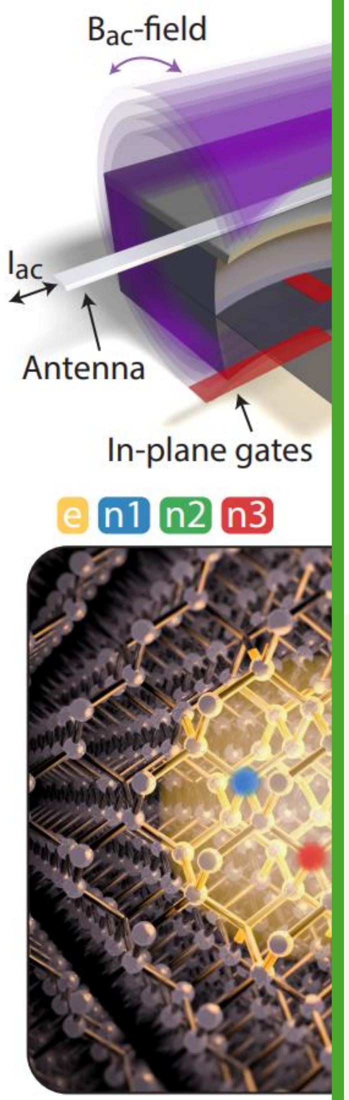

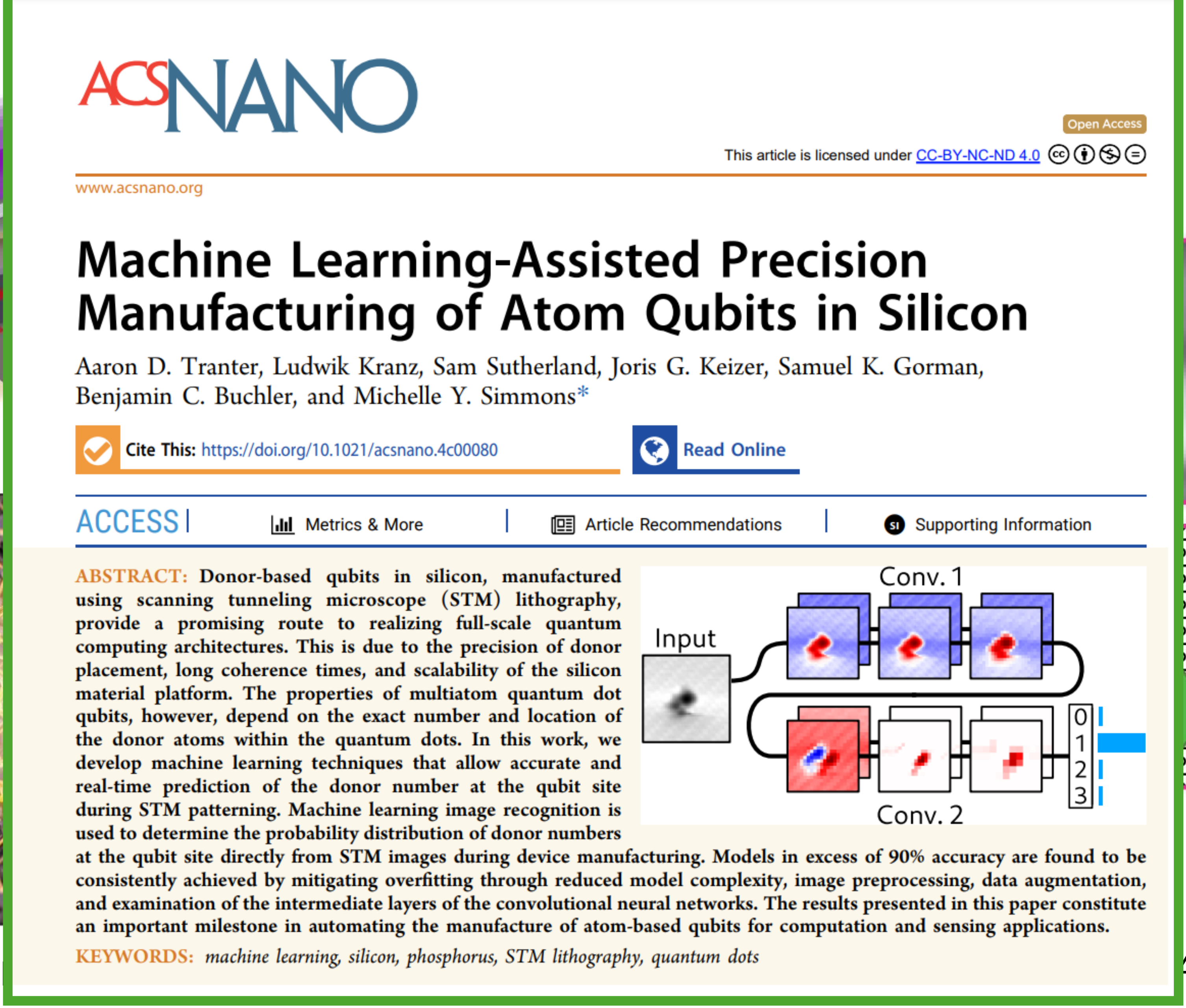

ACSNANO

Open Access

www.acsnano.org

Machine Learning-Assisted Precision Manufacturing of Atom Qubits in Silicon

Aaron D. Tranter, Ludwik Kranz, Sam Sutherland, Joris G. Keizer, Samuel K. Gorman, Benjamin C. Buchler, and Michelle Y. Simmons*

Cite This: https://doi.org/10.1021/acsnano.4c00080

Read Online

ACCESS | Metrics & More | Article Recommendations | Supporting Information

ABSTRACT: Donor-based qubits in silicon, manufactured using scanning tunneling microscope (STM) lithography, provide a promising route to realizing full-scale quantum computing architectures. This is due to the precision of donor placement, long coherence times, and scalability of the silicon material platform. The properties of multiatom quantum dot qubits, however, depend on the exact number and location of the donor atoms within the quantum dots. In this work, we develop machine learning techniques that allow accurate and real-time prediction of the donor number at the qubit site during STM patterning. Machine learning image recognition is used to determine the probability distribution of donor numbers at the qubit site directly from STM images during device manufacturing. Models in excess of 90% accuracy are found to be consistently achieved by mitigating overfitting through reduced model complexity, image preprocessing, data augmentation, and examination of the intermediate layers of the convolutional neural networks. The results presented in this paper constitute an important milestone in automating the manufacture of atom-based qubits for computation and sensing applications.

KEYWORDS: *machine learning, silicon, phosphorus, STM lithography, quantum dots*

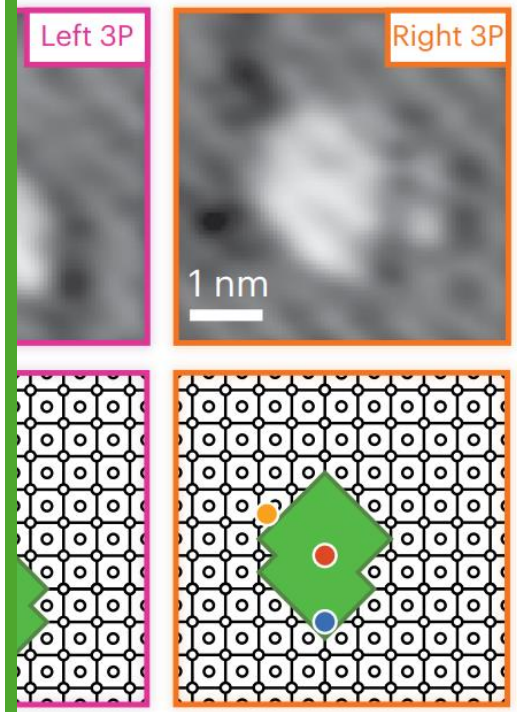

https://arxiv.org/

41565-023-01596-9

SCIENCE ADVANCES | RESEARCH ARTICLE

PHYSICS

Ramped measurement technique for robust high-fidelity spin qubit readout

Daniel Keith*, Yousun Chung, Ludwik Kranz, Brandur Thorgrimsson, Samuel K. Gorman, Michelle Y. Simmons

State preparation and measurement of single-electron spin qubits typically rely on spin-to-charge conversion where a spin-dependent charge transition of the electron is detected by a coupled charge sensor. For high-fidelity, fast readout, this process requires that the qubit energy is much larger than the temperature of the system limiting the temperature range for measurements. Here, we demonstrate an initialization and measurement technique that involves voltage ramps rather than static voltages allowing us to achieve state-to-charge readout fidelities above 99% for qubit energies almost half that required by traditional methods. This previously unidentified measurement technique is highly relevant for achieving high-fidelity electron spin readout at higher temperature operation and offers a number of pragmatic benefits compared to traditional energy-selective readout such as real-time dynamic feedback and minimal alignment procedures.

https://www.science.org/doi/10.1126/sciadv.abq0455

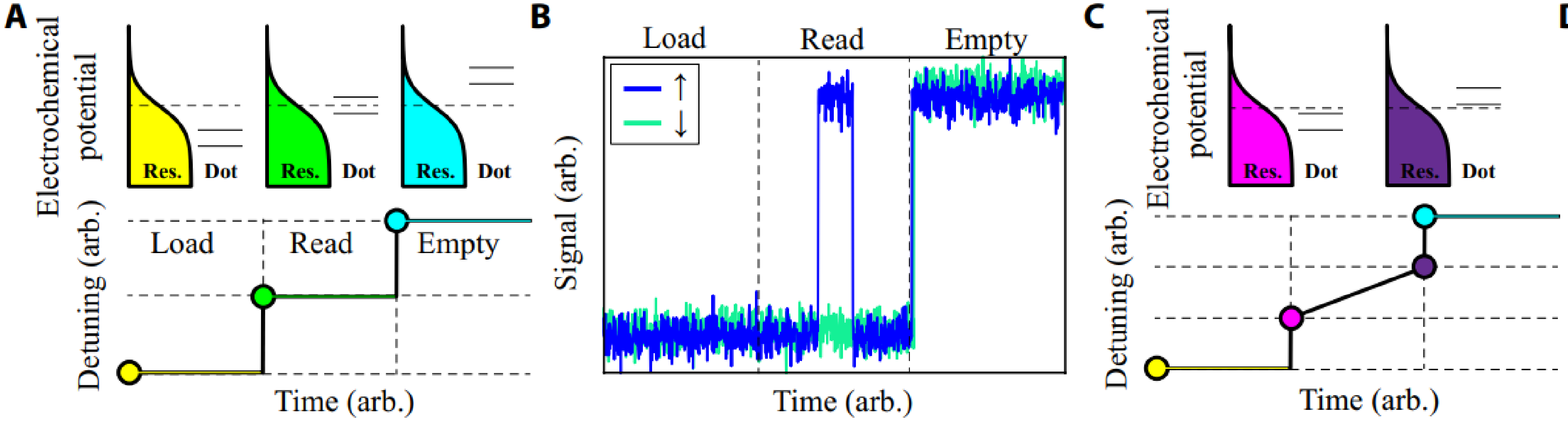

Fig. 1. Comparison of ESM and RSM techniques. (**A**) Electrochemical potential schematic for ESM and the corresponding voltage pulses used to align the electrochemical potentials of the electron spins to the Fermi level of the reservoir, E_F. The first pulse (yellow) loads an electron with a random spin state by moving both the electrochemical potentials, $\mu_{0\leftrightarrow\downarrow}$ and $\mu_{0\leftrightarrow\uparrow}$ below E_F. The spin state is then detected by a spin-dependent charge transition by moving E_F between $\mu_{0\leftrightarrow\downarrow}$ and $\mu_{0\leftrightarrow\uparrow}$ (green) such that only a spin-up electron will tunnel to the reservoir. A subsequent spin-down electron will then be loaded. Last, the electron is emptied by moving $\mu_{0\leftrightarrow\downarrow}$ and $\mu_{0\leftrightarrow\uparrow}$ above E_F (blue). (**B**) The corresponding signal from a nearby charge sensor during ESM. During the read phase, the spin-up state is detected as a characteristic blip in the charge sensor signal. (**C**) Electrochemical potential schematic for RSM. The load (yellow) and empty (blue) phases are the same as for ESM. During the read phase, the electrochemical potentials, $\mu_{0\leftrightarrow\downarrow}$ and $\mu_{0\leftrightarrow\uparrow}$, are continuously ramped from below E_F (pink) to above E_F (purple). (**D**) The corresponding charge sensor signal for RSM. A blip in the charge sensor signal before a certain threshold time indicates the presence of a spin-up electron. The charge sensor signal always reaches the maximum value before the empty phase as the spin-down electron will also tunnel out to the reservoir during the read phase.

https://www.science.org/doi/10.1126/sciadv.abq0455

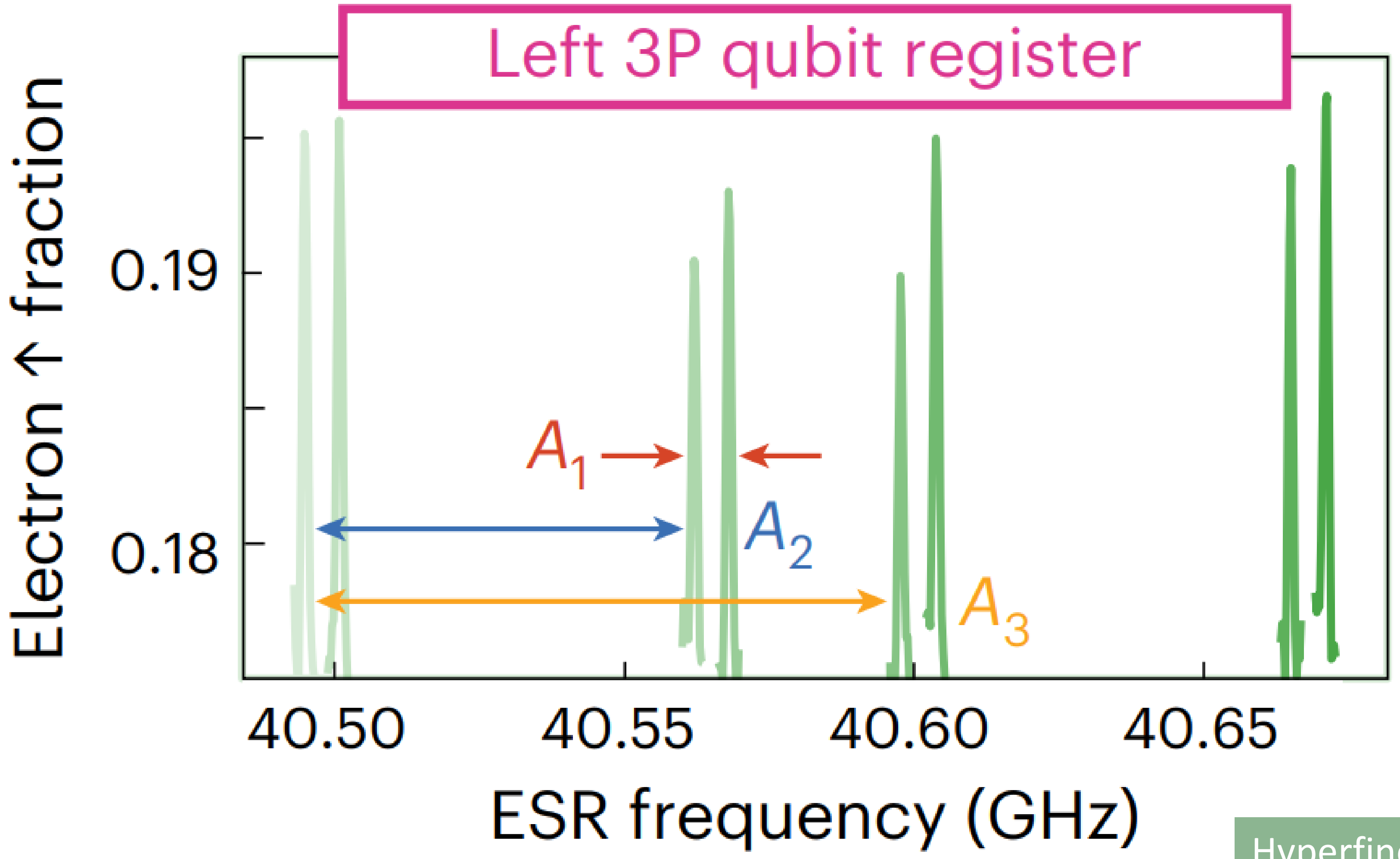

Hyperfine interaction strengths

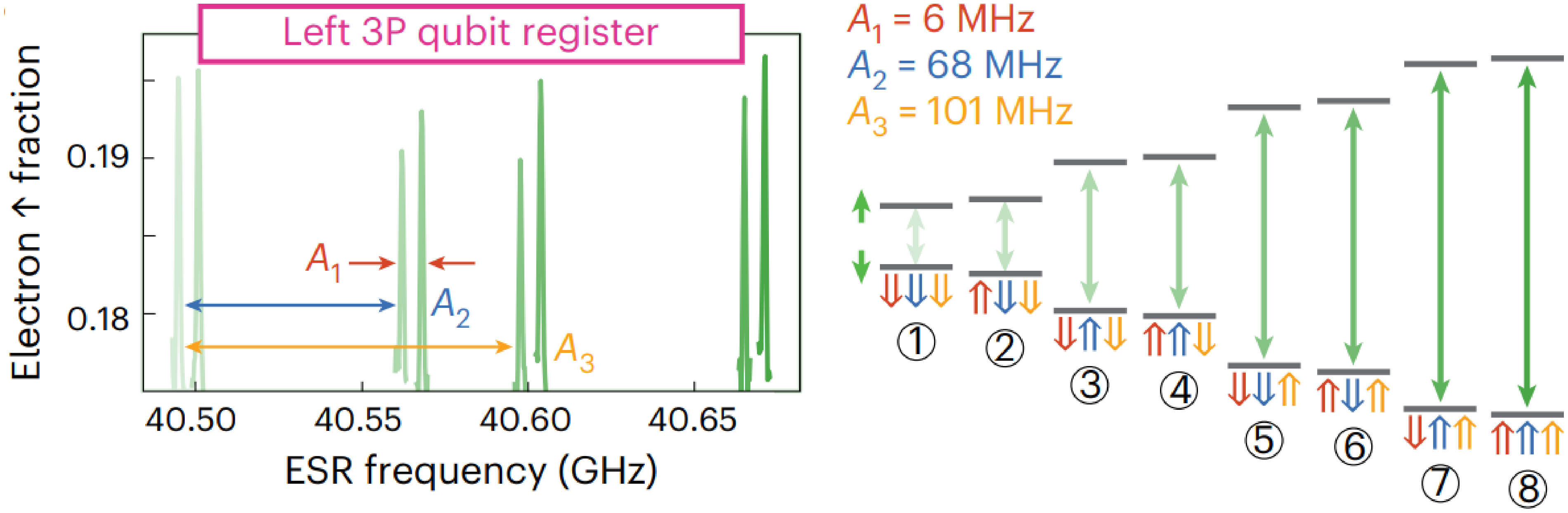

Hyperfine interaction strengths

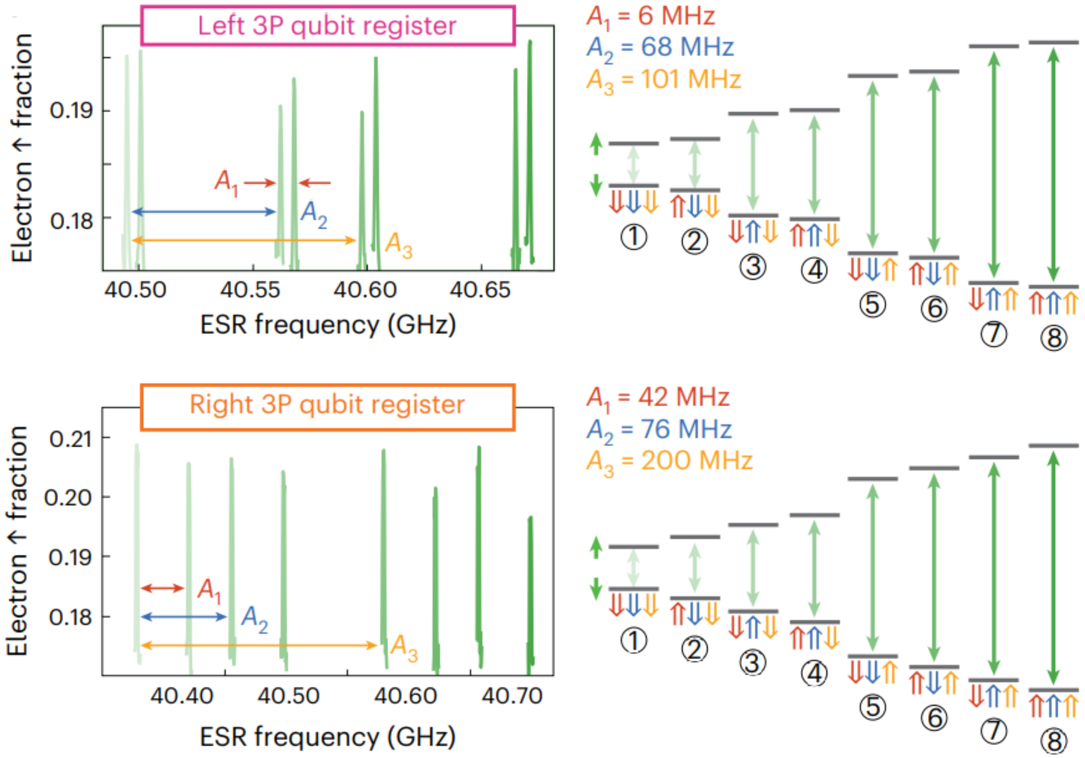

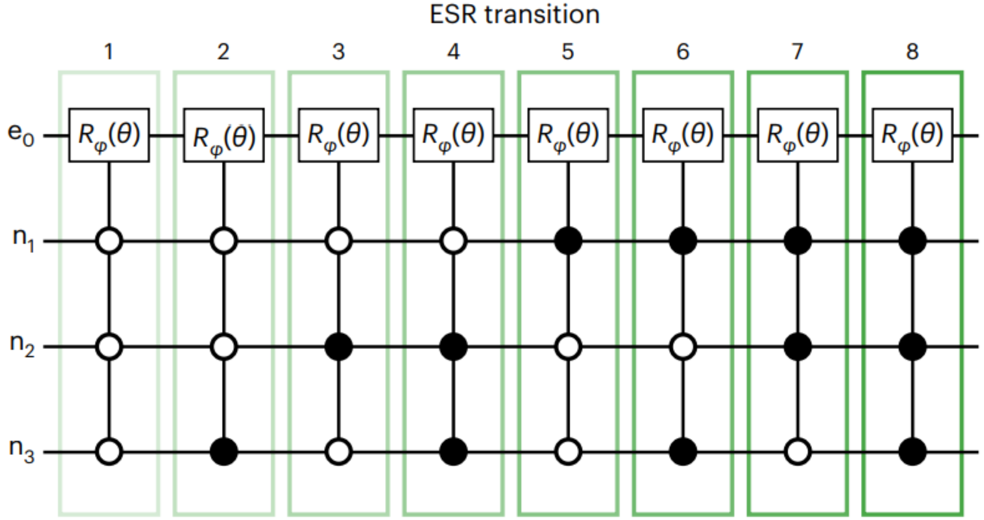

○ conditional on spin down

● conditional on spin up

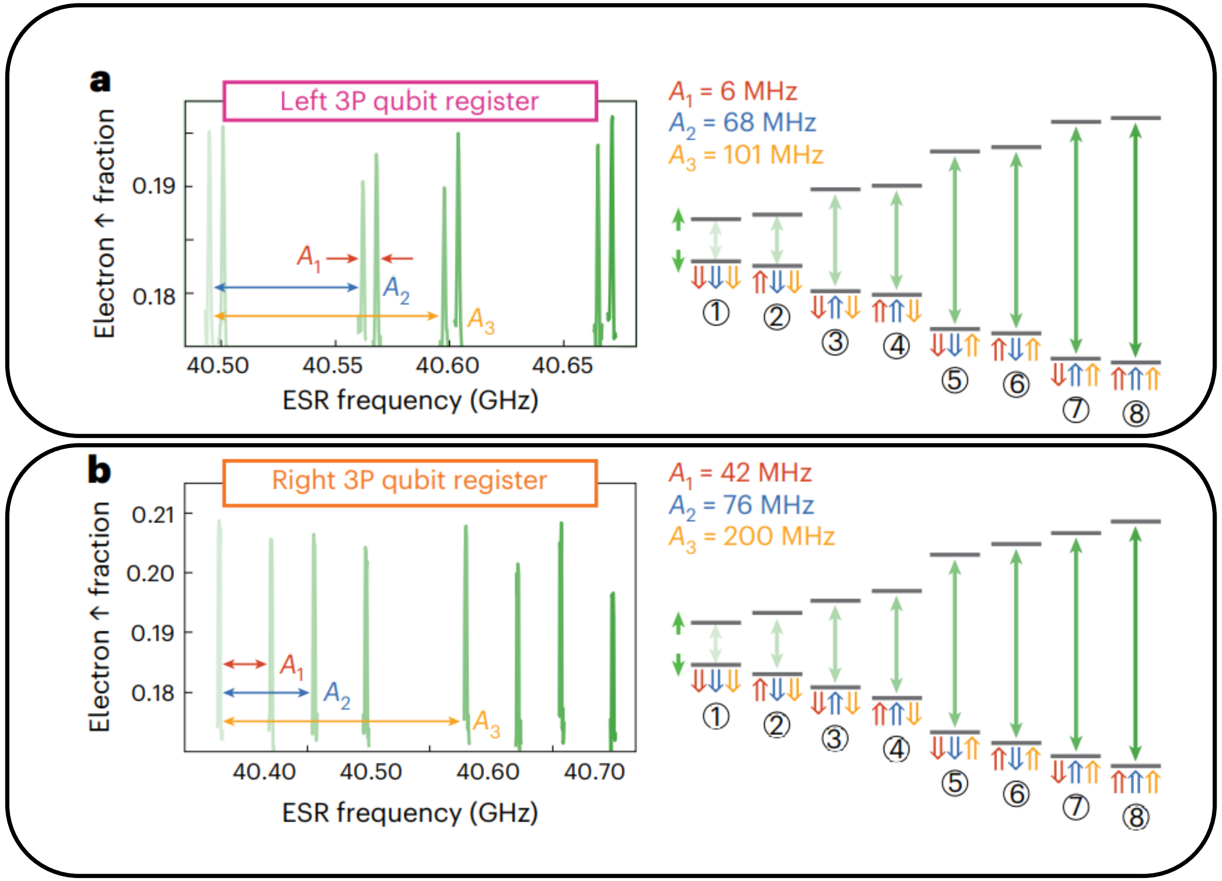

nature nanotechnology

Article

https://doi.org/10.1038/s41565-023-01596-9

High-fidelity initialization and control of electron and nuclear spins in a four-qubit register

Received: 10 August 2023

Accepted: 20 December 2023

Published online: 7 February 2024

J. Reiner[1,2,4], Y. Chung[1,2,4], S. H. Misha[1,2,4], C. Lehner[1,2], C. Moehle[1,2], D. Poulos[1,2], S. Monir[2,3], K. J. Charde[1,2], P. Macha[1,2], L. Kranz[1,2], I. Thorvaldson[1,2], B. Thorgrimsson[1,2], D. Keith[1,2], Y. L. Hsueh[2,3], R. Rahman[2,3], S. K. Gorman[1,2], J. G. Keizer[1,2] & M. Y. Simmons[1,2] ✉

ESR explanation

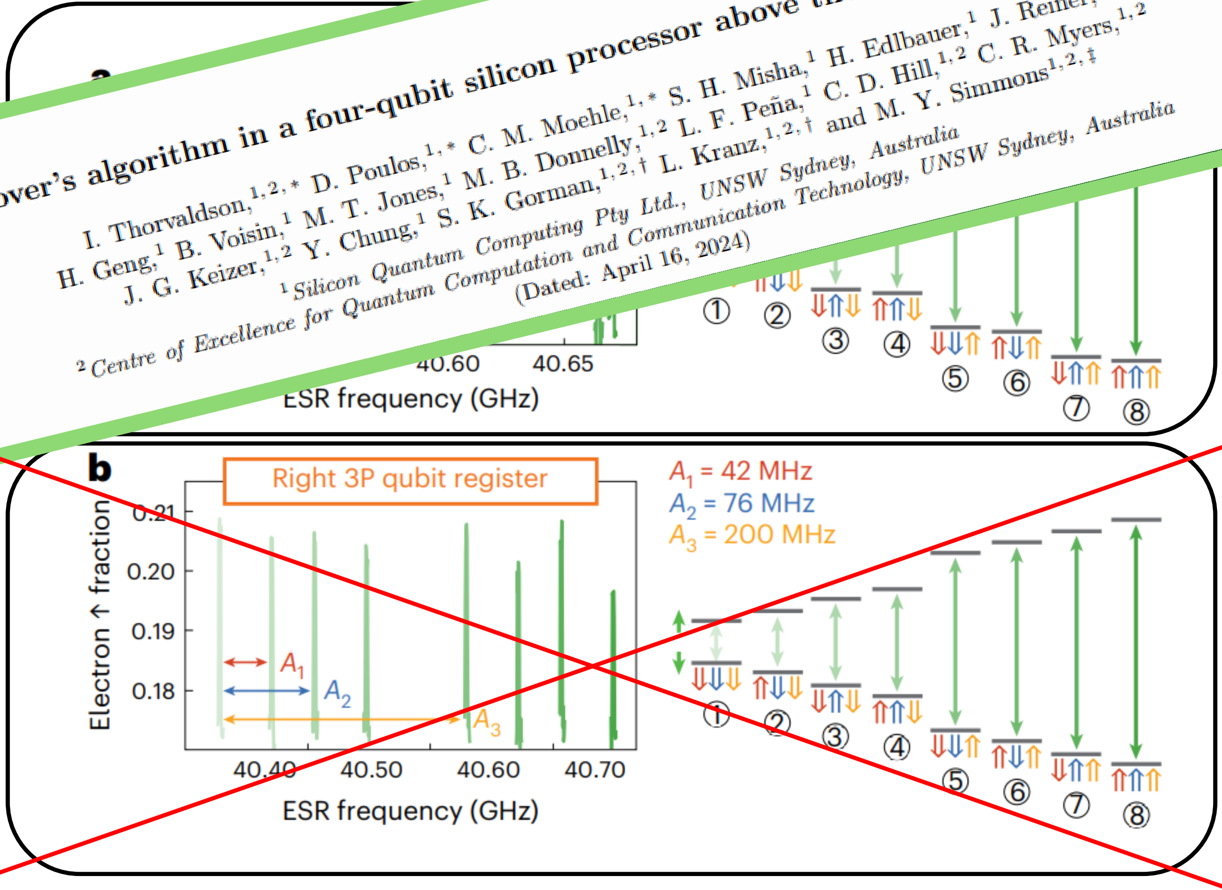

Grover's algorithm in a four-qubit silicon processor above the fault-tolerant threshold

I. Thorvaldson,[1,2,*] D. Poulos,[1,*] C. M. Moehle,[1,*] S. H. Misha,[1] H. Edlbauer,[1] J. Reiner,[1] H. Geng,[1] B. Voisin,[1] M. T. Jones,[1] M. B. Donnelly,[1,2] L. F. Peña,[1] C. D. Hill,[1,2] C. R. Myers,[1,2] J. G. Keizer,[1,2] Y. Chung,[1] S. K. Gorman,[1,2,†] L. Kranz,[1,2,†] and M. Y. Simmons[1,2,‡]

[1] *Silicon Quantum Computing Pty Ltd., UNSW Sydney, Australia*

[2] *Centre of Excellence for Quantum Computation and Communication Technology, UNSW Sydney, Australia*

(Dated: April 16, 2024)

nature nanotechnology

Article

https://doi.org/10.1038/s41565-023-01596-9

High-fidelity initialization and control of electron and nuclear spins in a four-qubit register

Received: 10 August 2023

Accepted: 20 December 2023

Published online: 7 February 2024

J. Reiner[1,2,4], Y. Chung[1,2,4], S. H. Misha[1,2,4], C. Lehner[1,2], C. Moehle[1,2], D. Poulos[1,2], S. Monir[2,3], K. J. Charde[1,2], P. Macha[1,2], L. Kranz[1,2], I. Thorvaldson[1,2], B. Thorgrimsson[1,2], D. Keith[1,2], Y. L. Hsueh[2,3], R. Rahman[2,3], S. K. Gorman[1,2], J. G. Keizer[1,2] & M. Y. Simmons[1,2] ✉

The same device – a new paper

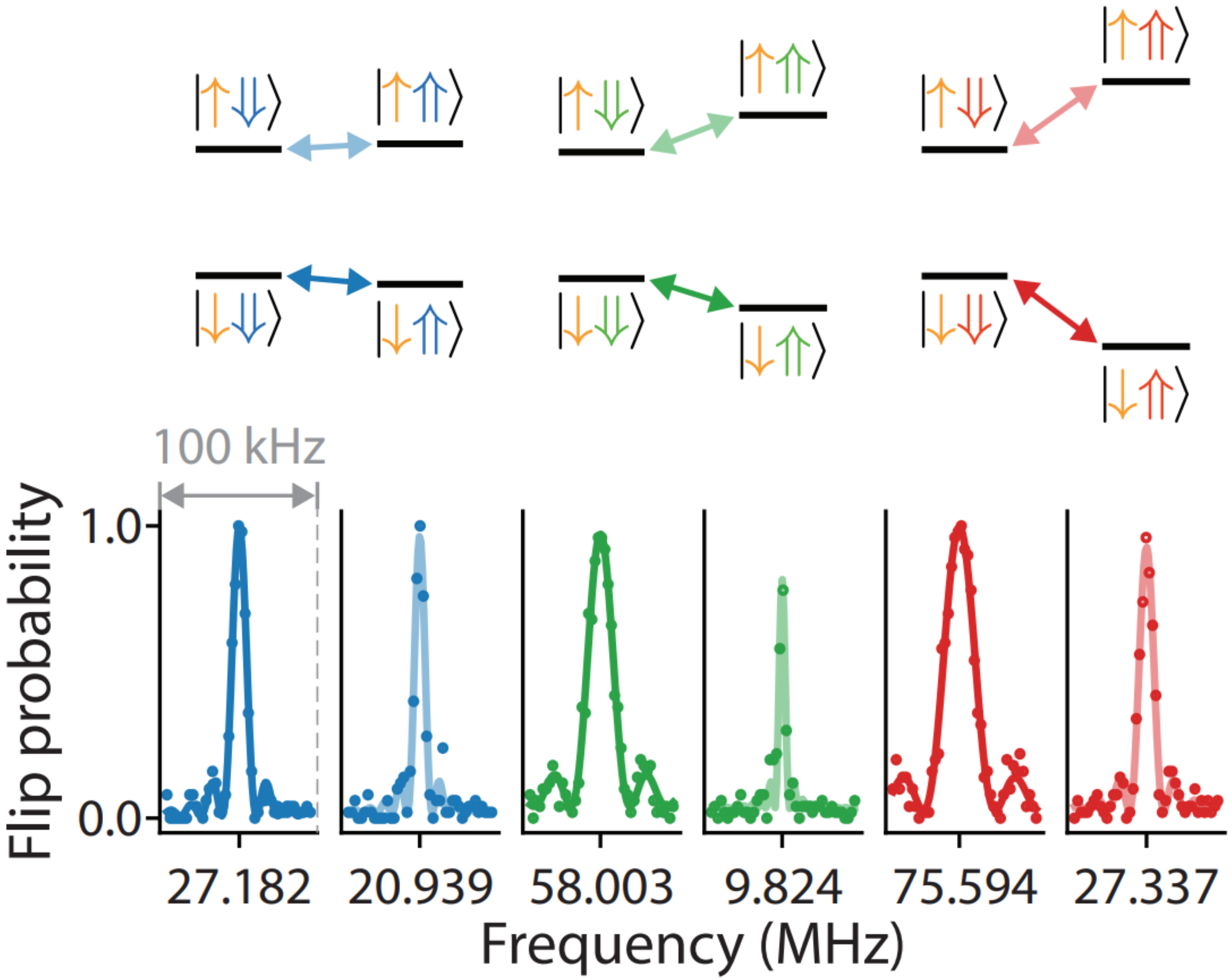

Frequency -> addressability to a specific qubit

https://www.nature.com/articles/s41565-023-01596-9

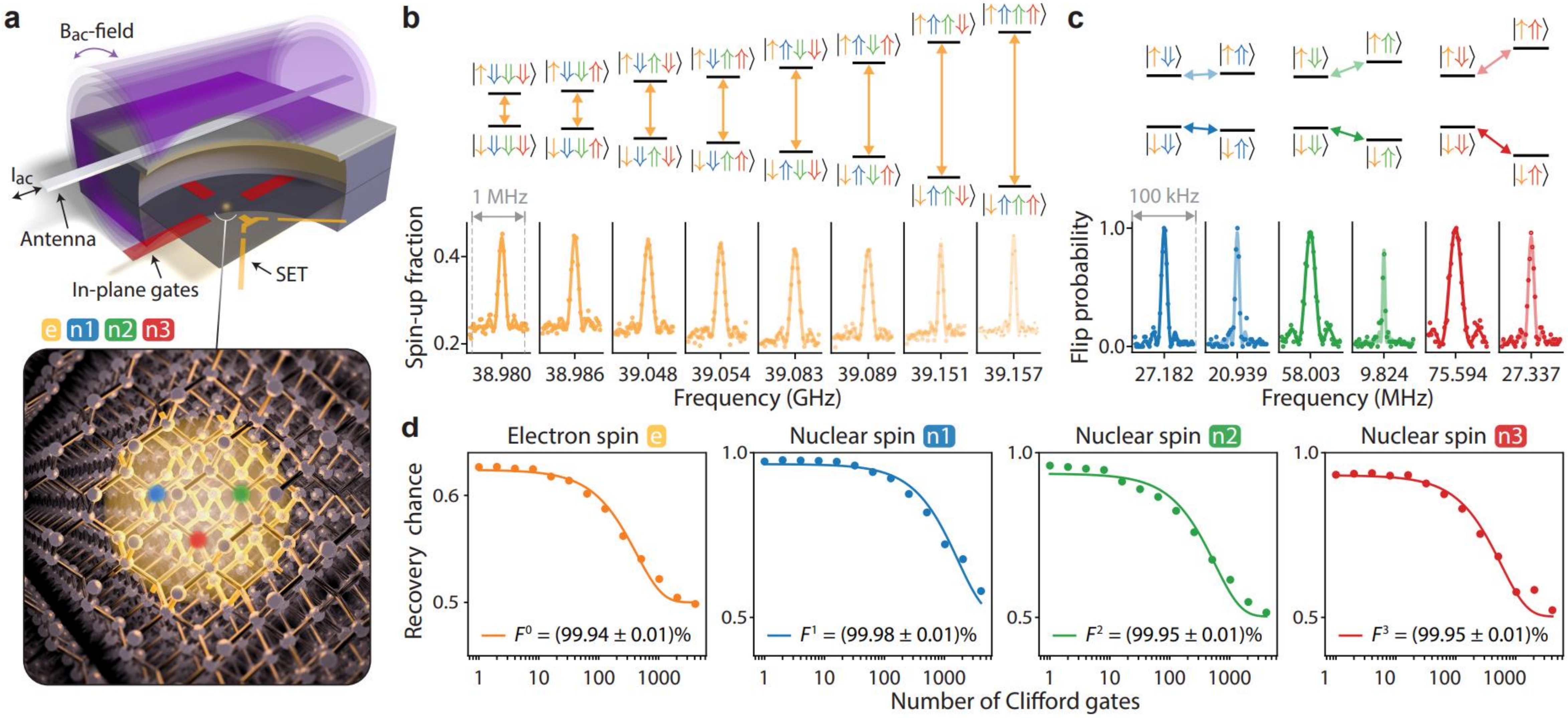

Single-qubit operations

$C_1 sin(\omega t + \phi) + C2$

Rabi oscillations

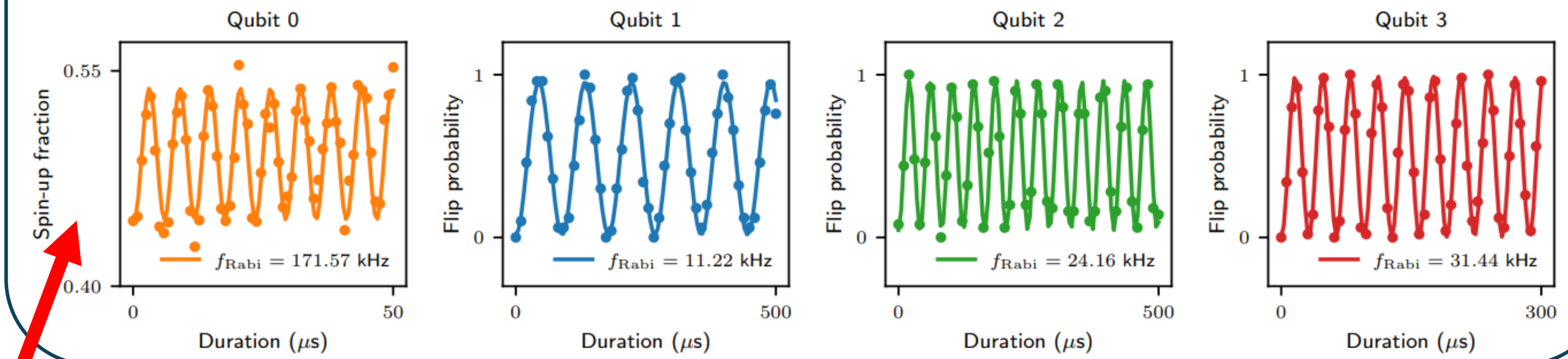

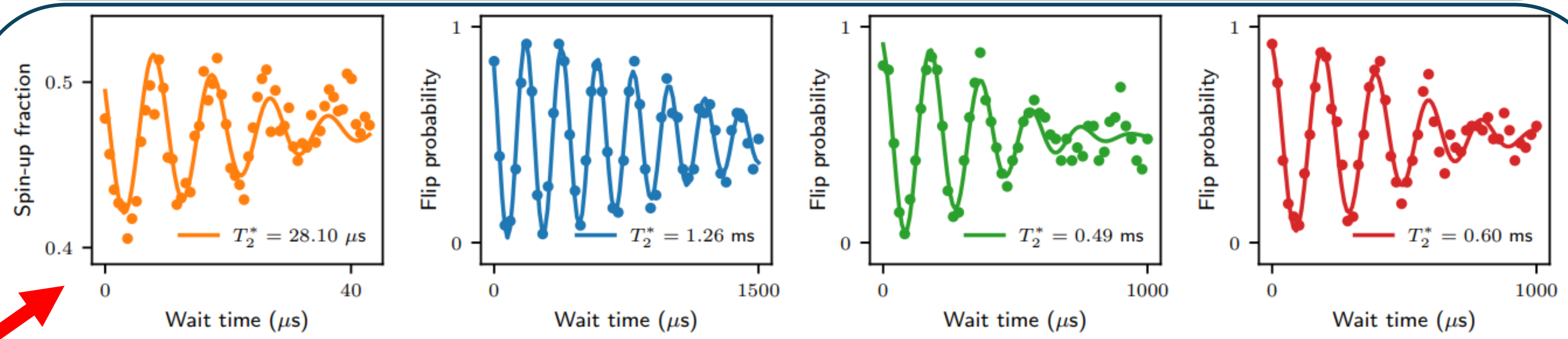

Nuclear state:

$|\Downarrow\Downarrow\Downarrow\Downarrow\rangle$

$$A\, sin(\omega t + \phi) \exp\left(-\left(\frac{t}{T_2}\right)^2\right) + B$$

Ramsey experiment

$C_1 sin(\omega t + \phi) + C2$

Rabi oscillations

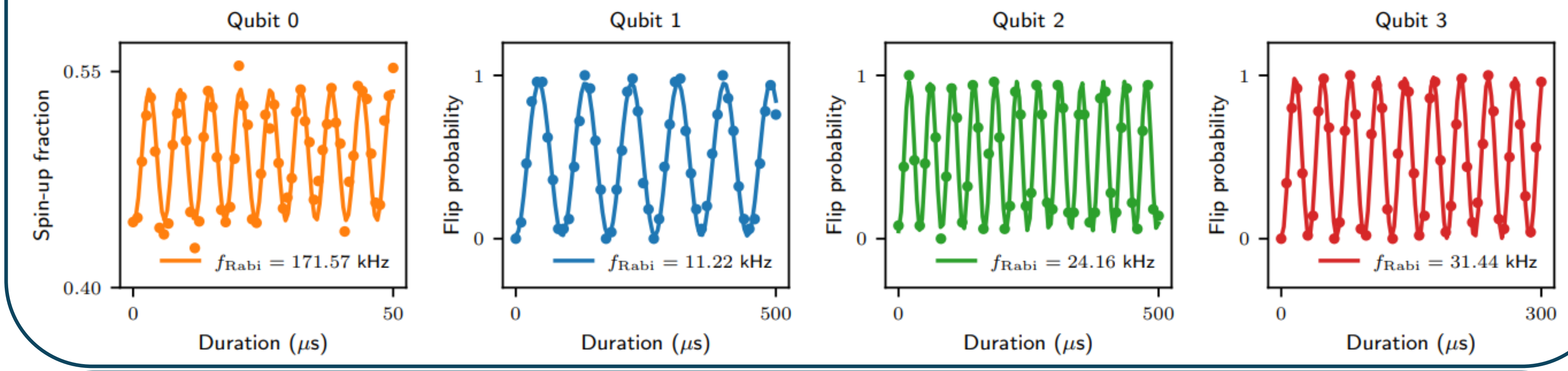

Rabi frequency and dephasing time
for the **electron spin qubit**
with the nuclear spins initialized
into the different configurations as depicted

Nuclear spin state	f_{Rabi} (kHz)	T_2^* (μs)
$\lvert\Downarrow\Downarrow\Downarrow\rangle$	171.57	28.10
$\lvert\Downarrow\Downarrow\Uparrow\rangle$	170.67	31.43
$\lvert\Downarrow\Uparrow\Downarrow\rangle$	172.27	33.60
$\lvert\Downarrow\Uparrow\Uparrow\rangle$	172.01	30.79
$\lvert\Uparrow\Downarrow\Downarrow\rangle$	168.63	26.71
$\lvert\Uparrow\Downarrow\Uparrow\rangle$	171.04	38.26
$\lvert\Uparrow\Uparrow\Downarrow\rangle$	170.64	37.75
$\lvert\Uparrow\Uparrow\Uparrow\rangle$	171.29	26.73

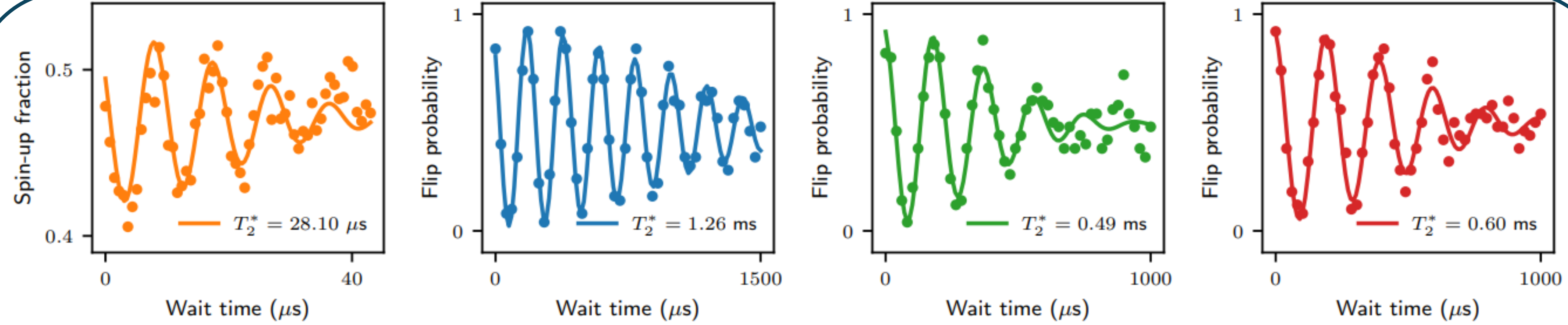

$$A\, sin(\omega t + \phi)\exp\left(-\left(\frac{t}{T_2}\right)^2\right) + B$$

Ramsey experiment

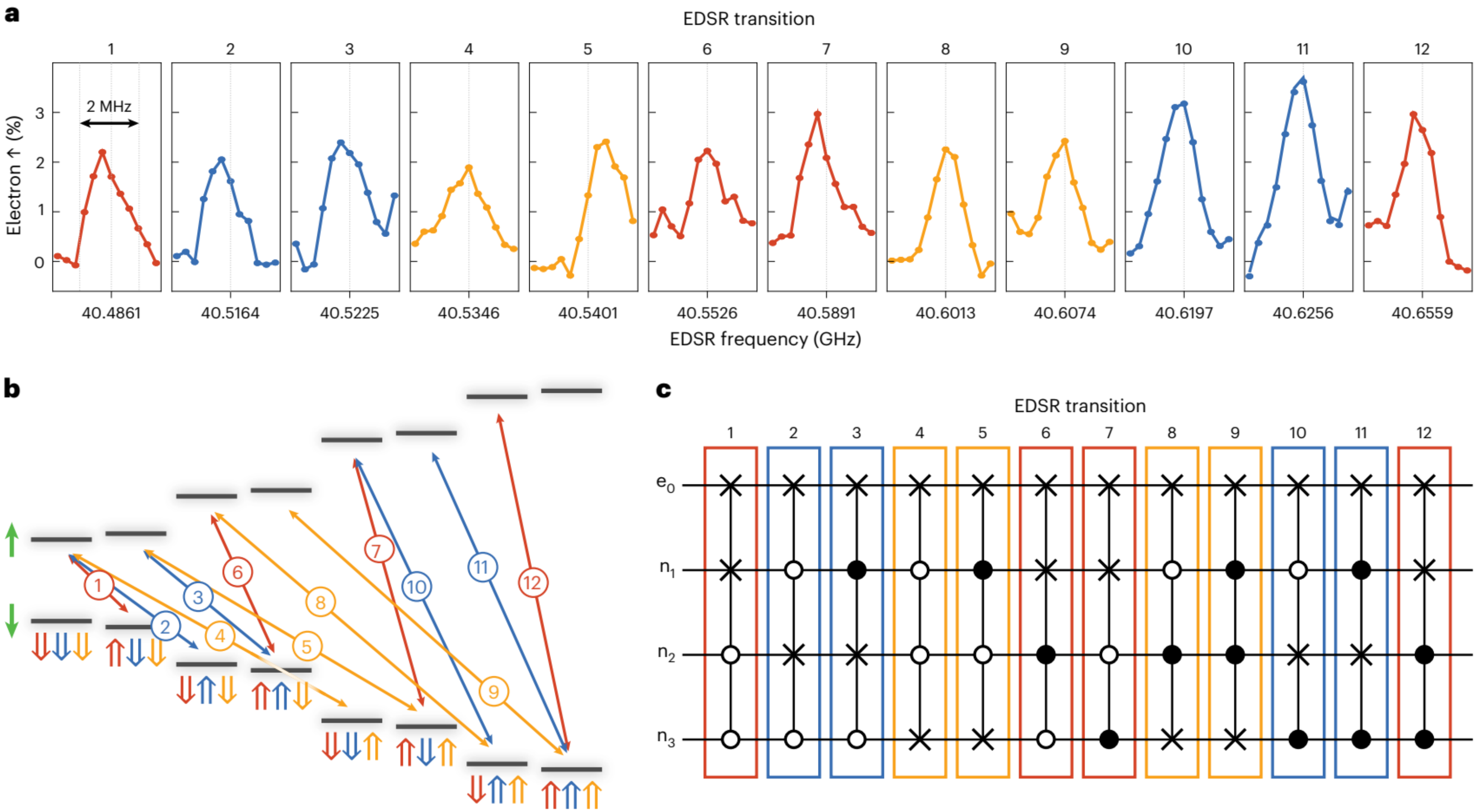

○ conditional on spin down

● conditional on spin up

✖ spin flip-flops

EDSR explanation

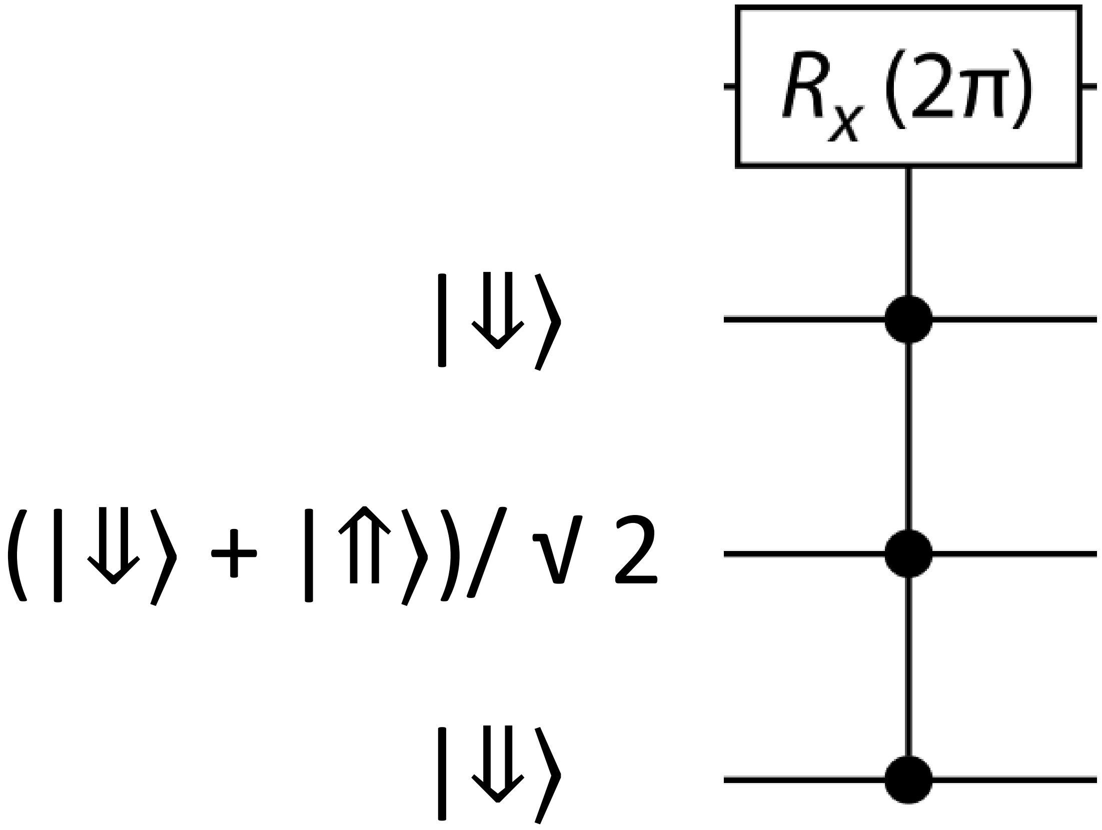

Berry phase for a spin ½ in the magnetic field

$\gamma = \frac{2\pi}{2} = \pi$

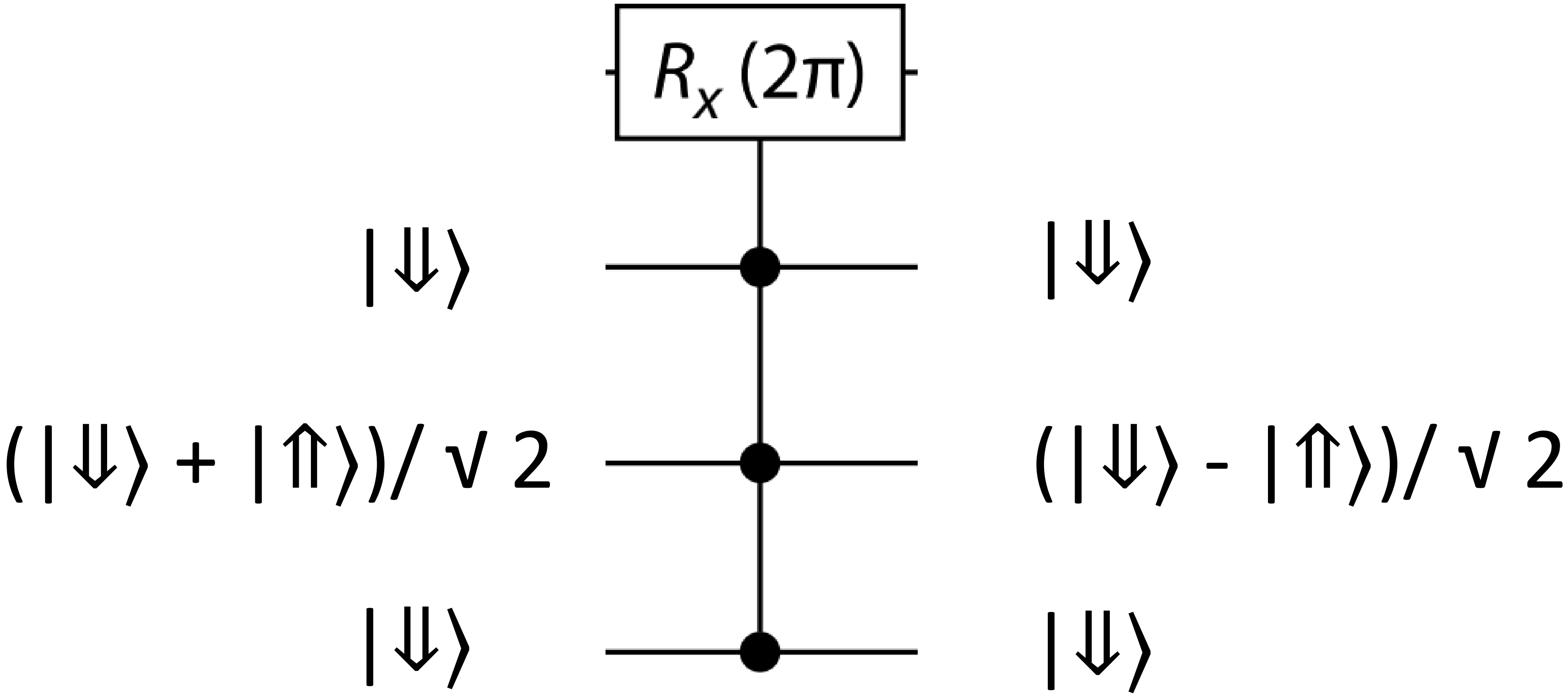
$R_x\,(2\pi)$
$|\Downarrow\rangle$
$(|\Downarrow\rangle + |\Uparrow\rangle)/\sqrt{2}$
$|\Downarrow\rangle$
$|\Downarrow\rangle$
$(|\Downarrow\rangle - |\Uparrow\rangle)/\sqrt{2}$
$|\Downarrow\rangle$

CZ gate

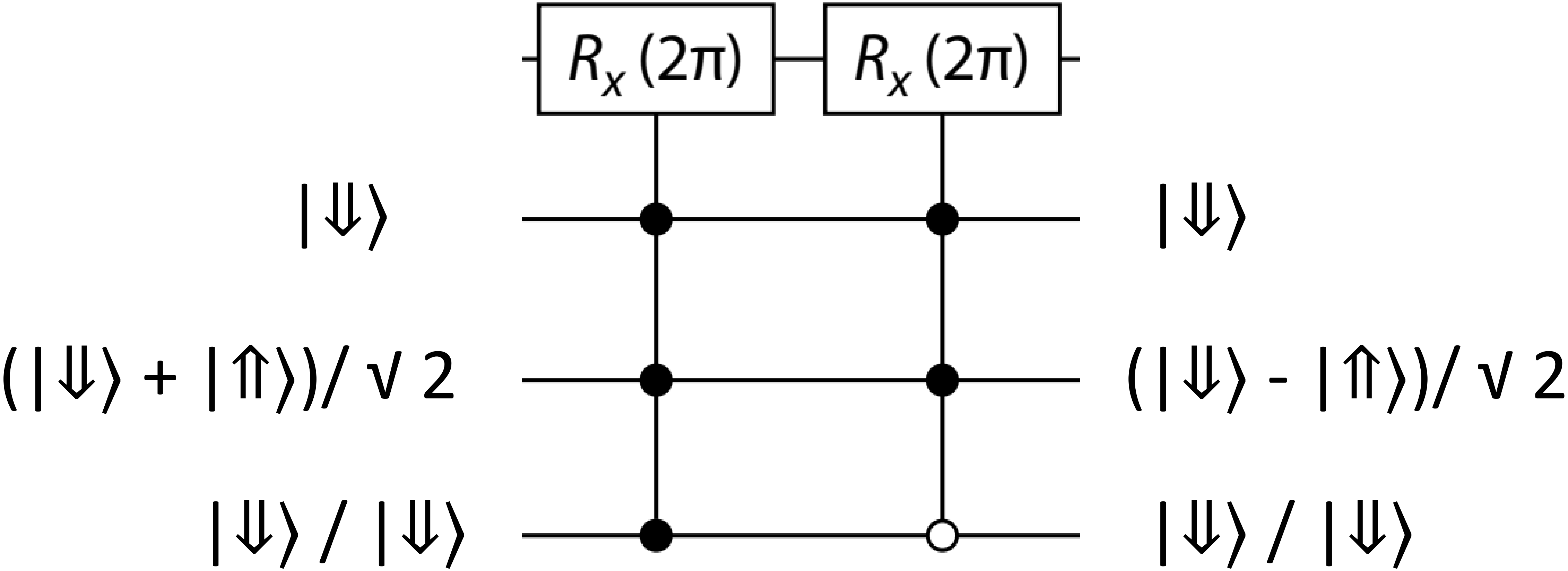
$R_x(2\pi)$
$R_x(2\pi)$
$|\Downarrow\rangle$
$(|\Downarrow\rangle + |\Uparrow\rangle)/\sqrt{2}$
$|\Downarrow\rangle / |\Downarrow\rangle$
$|\Downarrow\rangle$
$(|\Downarrow\rangle - |\Uparrow\rangle)/\sqrt{2}$
$|\Downarrow\rangle / |\Downarrow\rangle$

CZ gate

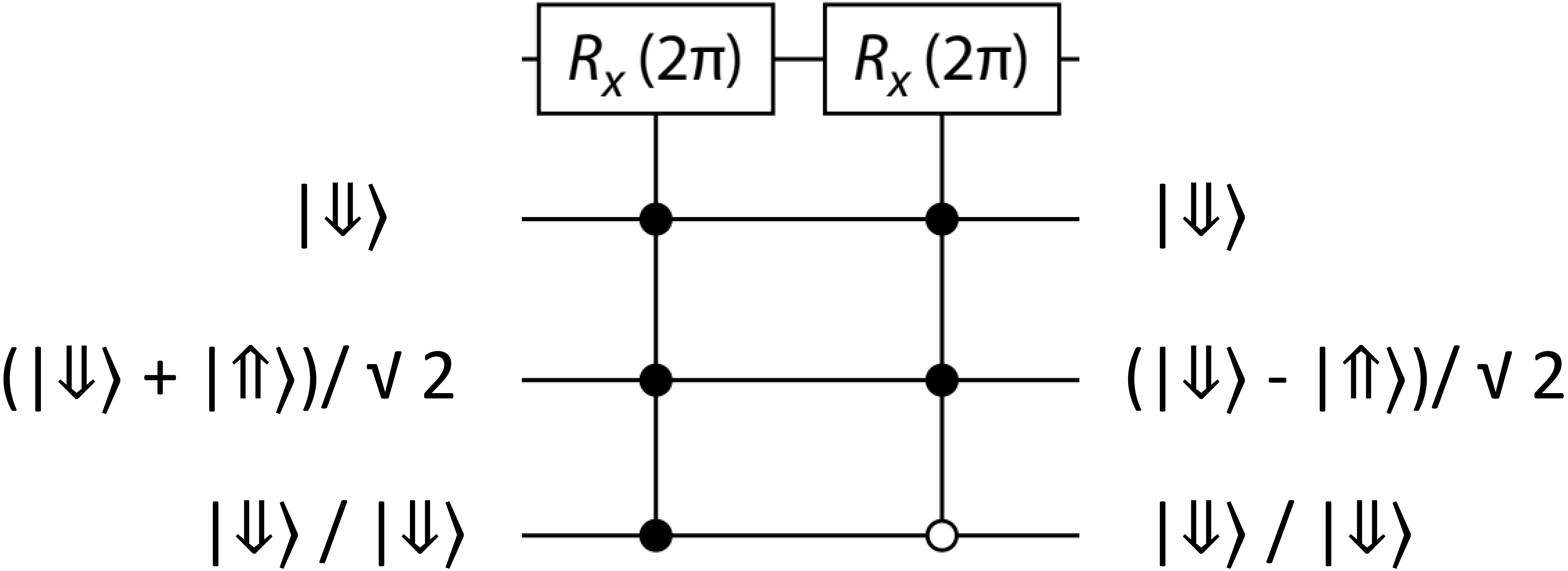
$R_x(2\pi)$
$R_x(2\pi)$
$|\Downarrow\rangle$
$(|\Downarrow\rangle + |\Uparrow\rangle)/\sqrt{2}$
$|\Downarrow\rangle / |\Downarrow\rangle$
$|\Downarrow\rangle$
$(|\Downarrow\rangle - |\Uparrow\rangle)/\sqrt{2}$
$|\Downarrow\rangle / |\Downarrow\rangle$

CZ gate

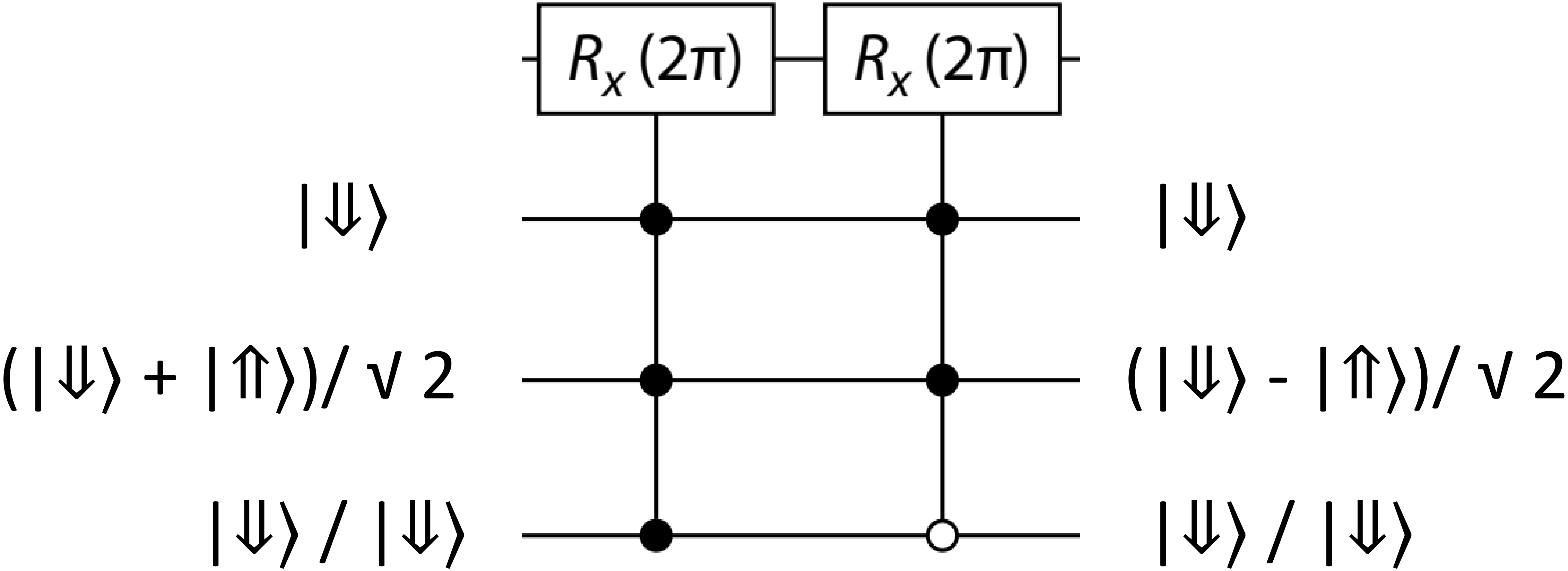

$R_x(2\pi)$
$R_x(2\pi)$
$|\Downarrow\rangle$
$(|\Downarrow\rangle + |\Uparrow\rangle)/\sqrt{2}$
$|\Downarrow\rangle / |\Downarrow\rangle$
$|\Downarrow\rangle$
$(|\Downarrow\rangle - |\Uparrow\rangle)/\sqrt{2}$
$|\Downarrow\rangle / |\Downarrow\rangle$

CNOT gate

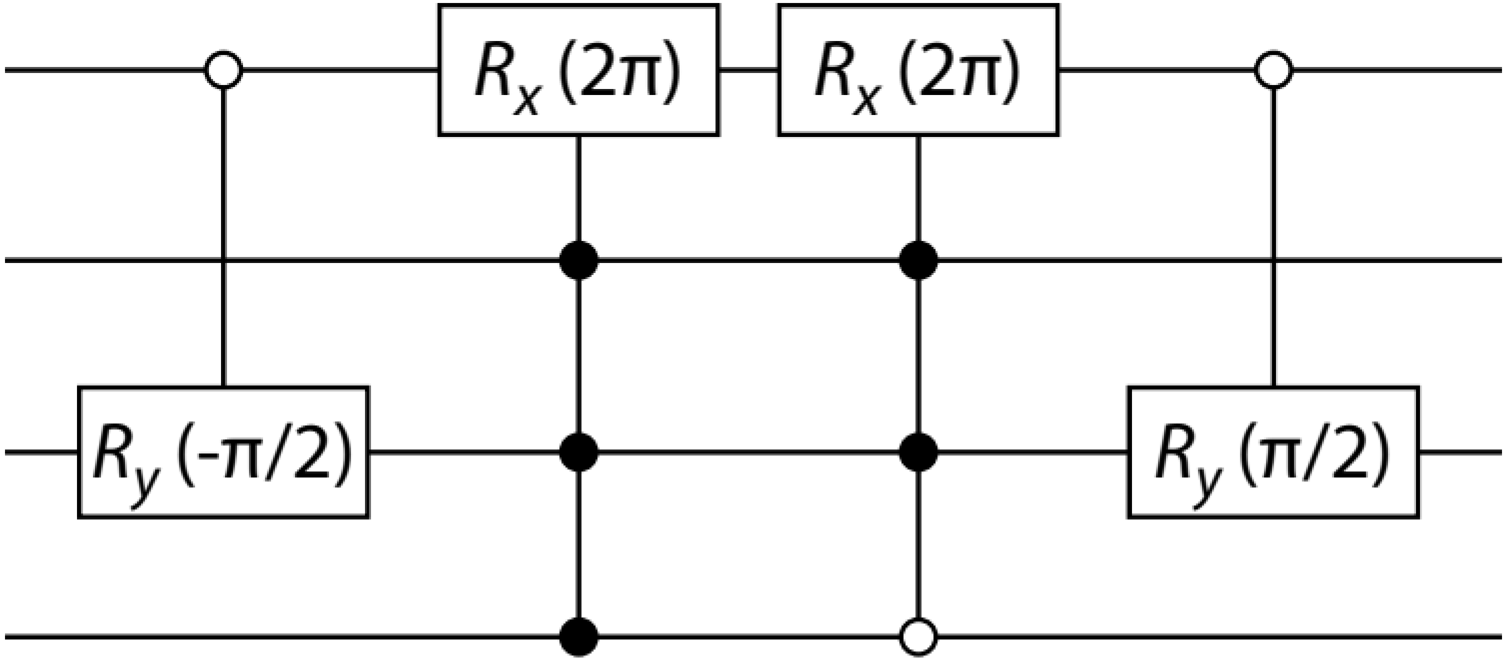

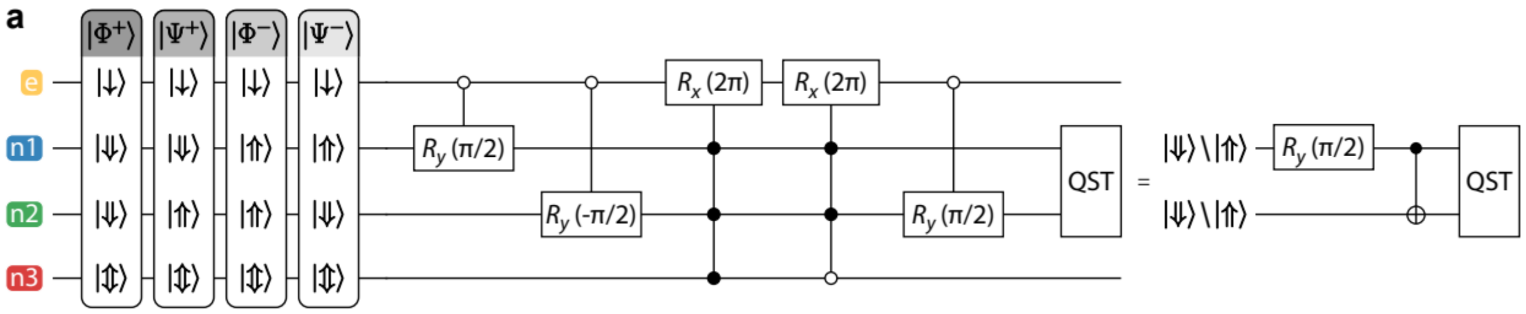

b

	F^{12}_{BS} (%)
$\|\Phi^+\rangle$	97.3 ± 0.7
$\|\Psi^+\rangle$	97.2 ± 0.5
$\|\Phi^-\rangle$	98.4 ± 0.5
$\|\Psi^-\rangle$	96.7 ± 0.7
Avg.	97.5 ± 0.3

c

	F^{13}_{BS} (%)
$\|\Phi^+\rangle$	97.2 ± 0.7
$\|\Psi^+\rangle$	98.1 ± 0.6
$\|\Phi^-\rangle$	97.8 ± 0.6
$\|\Psi^-\rangle$	97.5 ± 0.6
Avg.	97.7 ± 0.4

d

	F^{23}_{BS} (%)
$\|\Phi^+\rangle$	96.7 ± 0.7
$\|\Psi^+\rangle$	95.6 ± 0.8
$\|\Phi^-\rangle$	98.0 ± 0.6
$\|\Psi^-\rangle$	96.0 ± 0.7
Avg.	96.8 ± 0.4

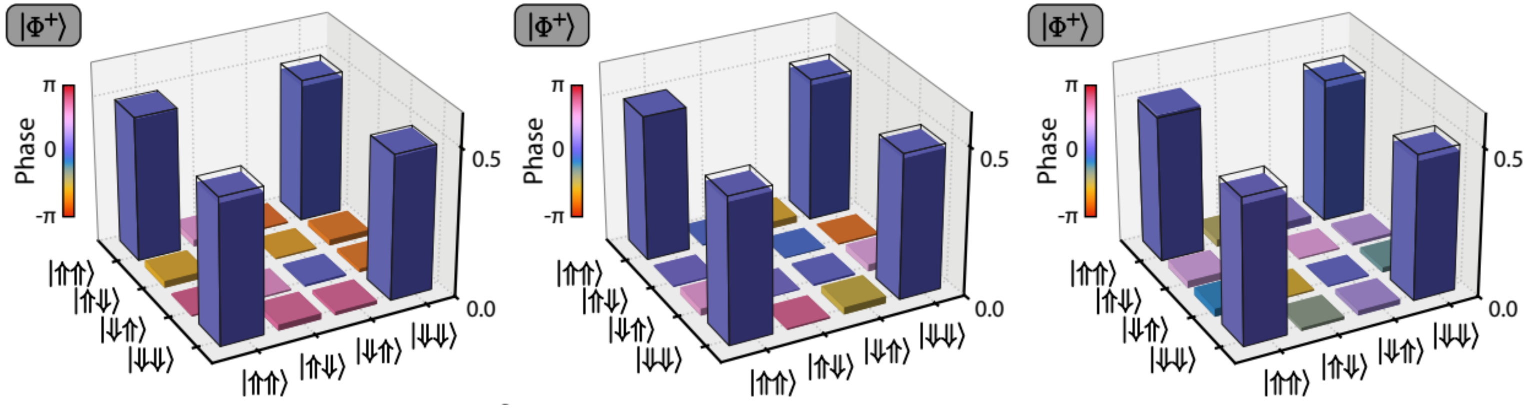

Bell states tomography

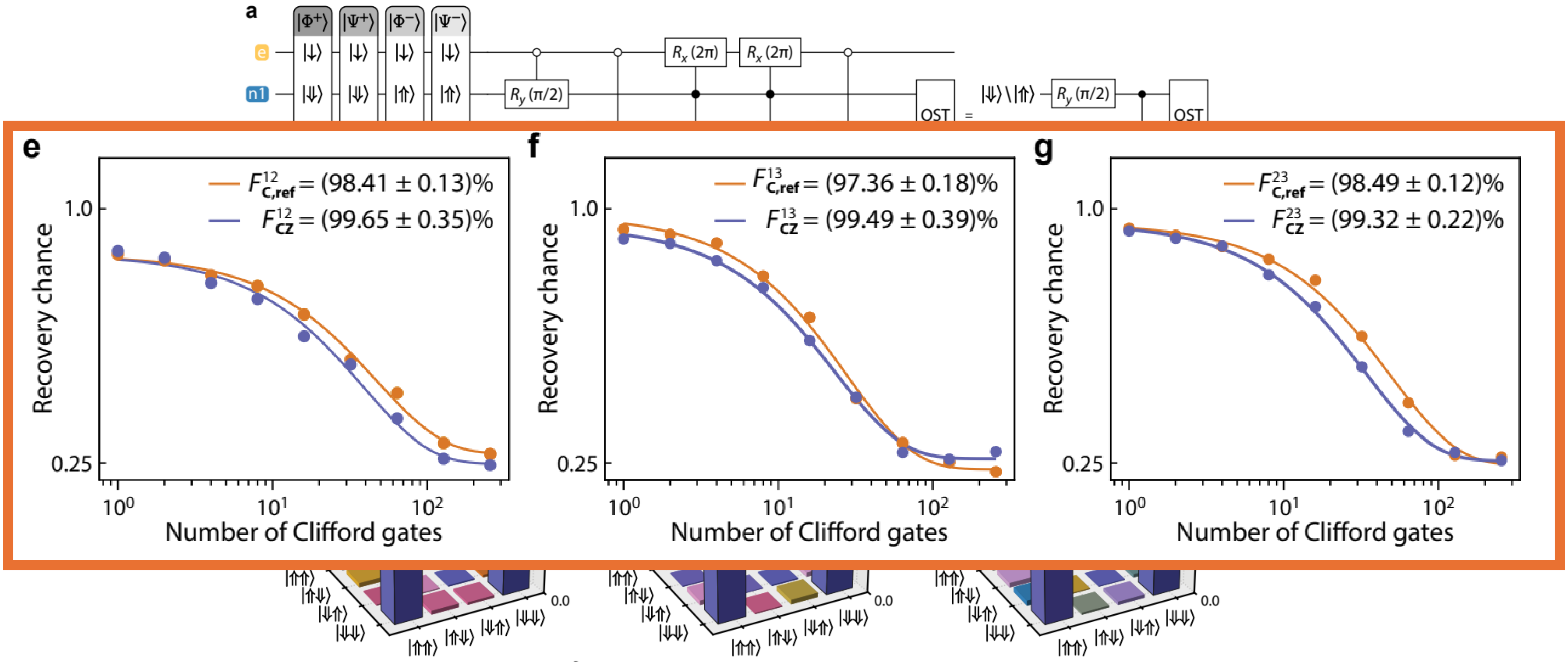

a
|Φ⁺⟩
|Ψ⁺⟩
|Φ⁻⟩
|Ψ⁻⟩
e
n1
R_y (π/2)
R_x (2π)
R_x (2π)
OST
=
|⇓⟩ \ |⇑⟩
R_y (π/2)
OST
e
f
g
$F^{12}_{C,ref} = (98.41 \pm 0.13)\%$
$F^{12}_{CZ} = (99.65 \pm 0.35)\%$
$F^{13}_{C,ref} = (97.36 \pm 0.18)\%$
$F^{13}_{CZ} = (99.49 \pm 0.39)\%$
$F^{23}_{C,ref} = (98.49 \pm 0.12)\%$
$F^{23}_{CZ} = (99.32 \pm 0.22)\%$
Recovery chance
1.0
0.25
10^0
10^1
10^2
Number of Clifford gates
0.0
|⇑⇑⟩
|⇑⇓⟩
|⇓⇑⟩
|⇓⇓⟩

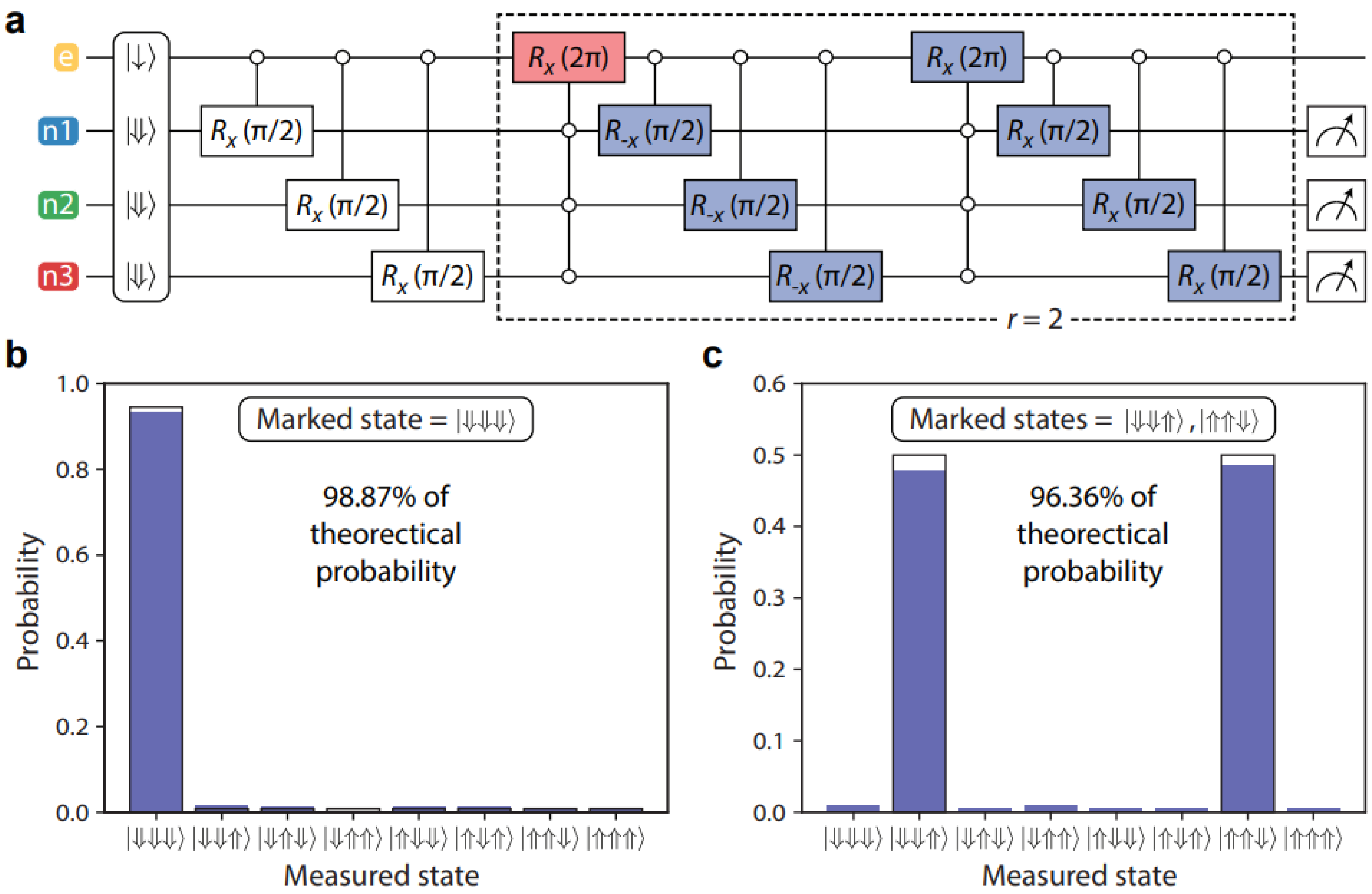
a
e
n1
n2
n3
$|\downarrow\rangle$
$|\Downarrow\rangle$
$R_x(\pi/2)$
$R_x(2\pi)$
$R_{-x}(\pi/2)$
$r = 2$
b
Marked state = $|\Downarrow\Downarrow\Downarrow\rangle$
98.87% of theoretical probability
Probability
Measured state
c
Marked states = $|\Downarrow\Downarrow\Uparrow\rangle$, $|\Uparrow\Uparrow\Downarrow\rangle$
96.36% of theoretical probability
Probability
Measured state

Outcome

- Quantum non-demolition readout – ramped technique

- ESR and NMR of all qubits in the 4q processor -> Single qubit operations

- Hyperfine interaction -> 2-3q entanglement:

  CZ gate
  CNOT gate

  Bell states + tomography
  ~~**GHZ** state~~ (not discussed here)

- **Grover's** algorithm

Electron spin initialization and readout is performed using a ramped spin measurement, giving a fidelity of ~81% at an electron temperature of ~200 mK at magnetic field B = 1.45 T.

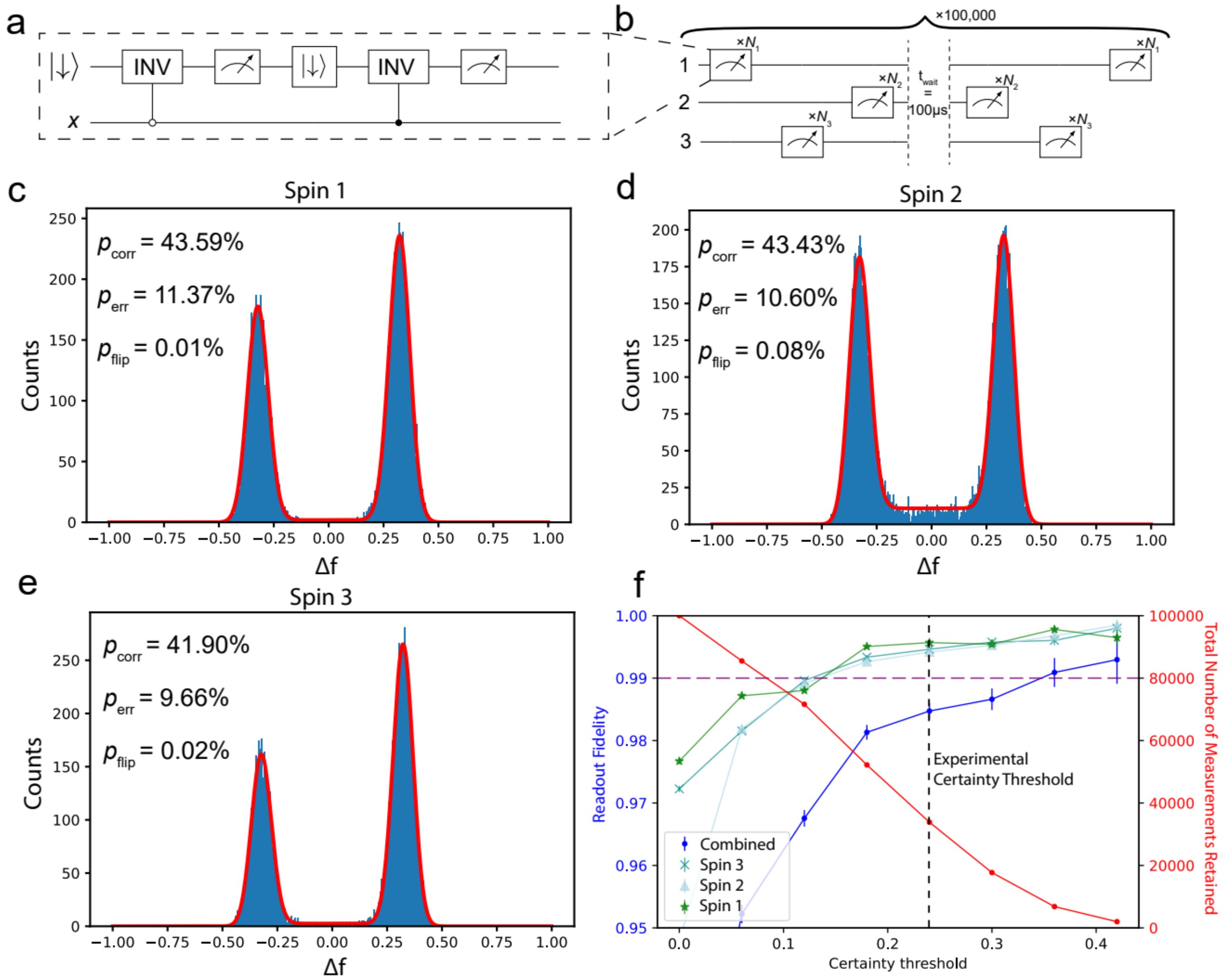

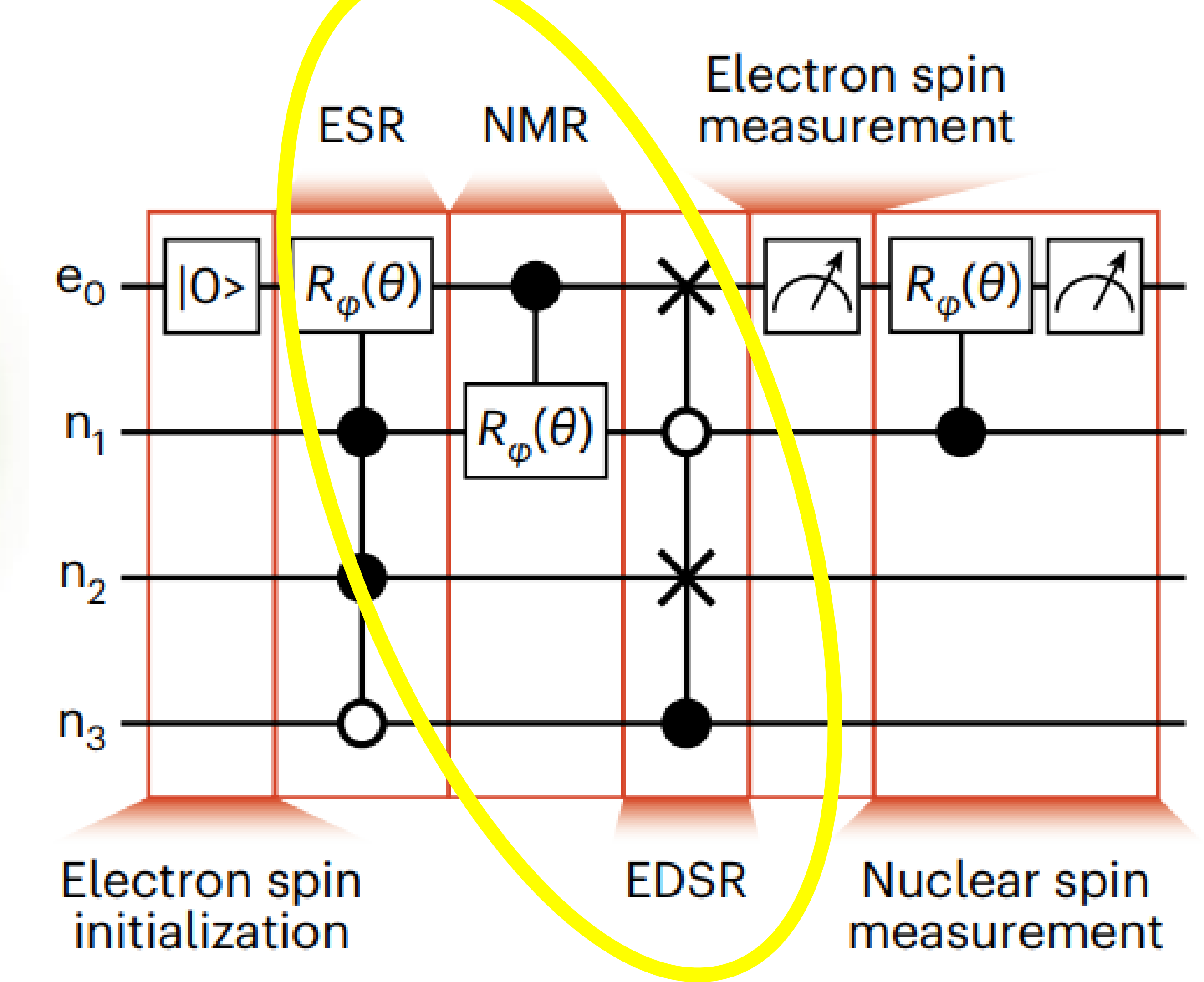
ESR
NMR
Electron spin measurement
e_0
n_1
n_2
n_3
|0>
$R_\varphi(\theta)$
$R_\varphi(\theta)$
$R_\varphi(\theta)$
Electron spin initialization
EDSR
Nuclear spin measurement

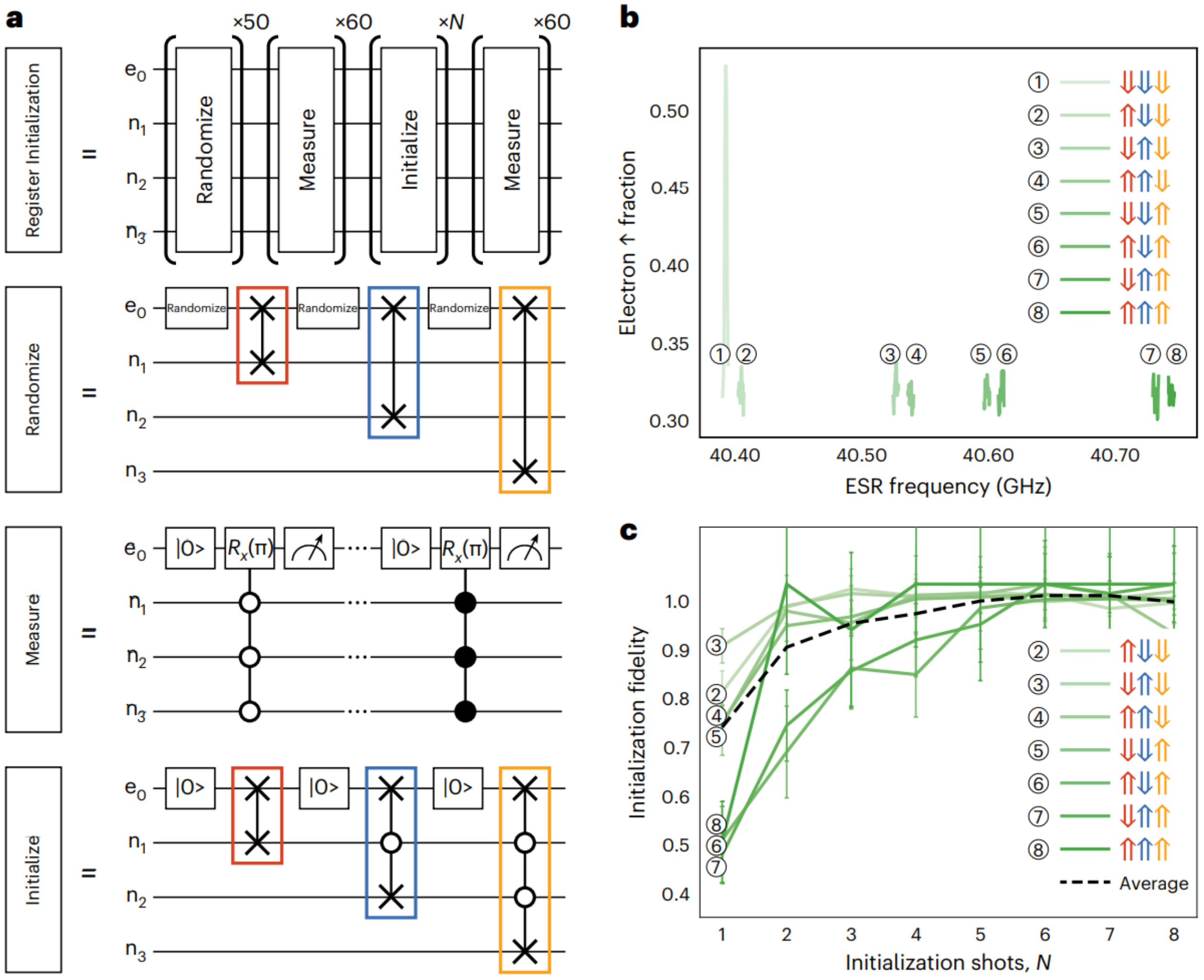

ESR explanation, **Index**

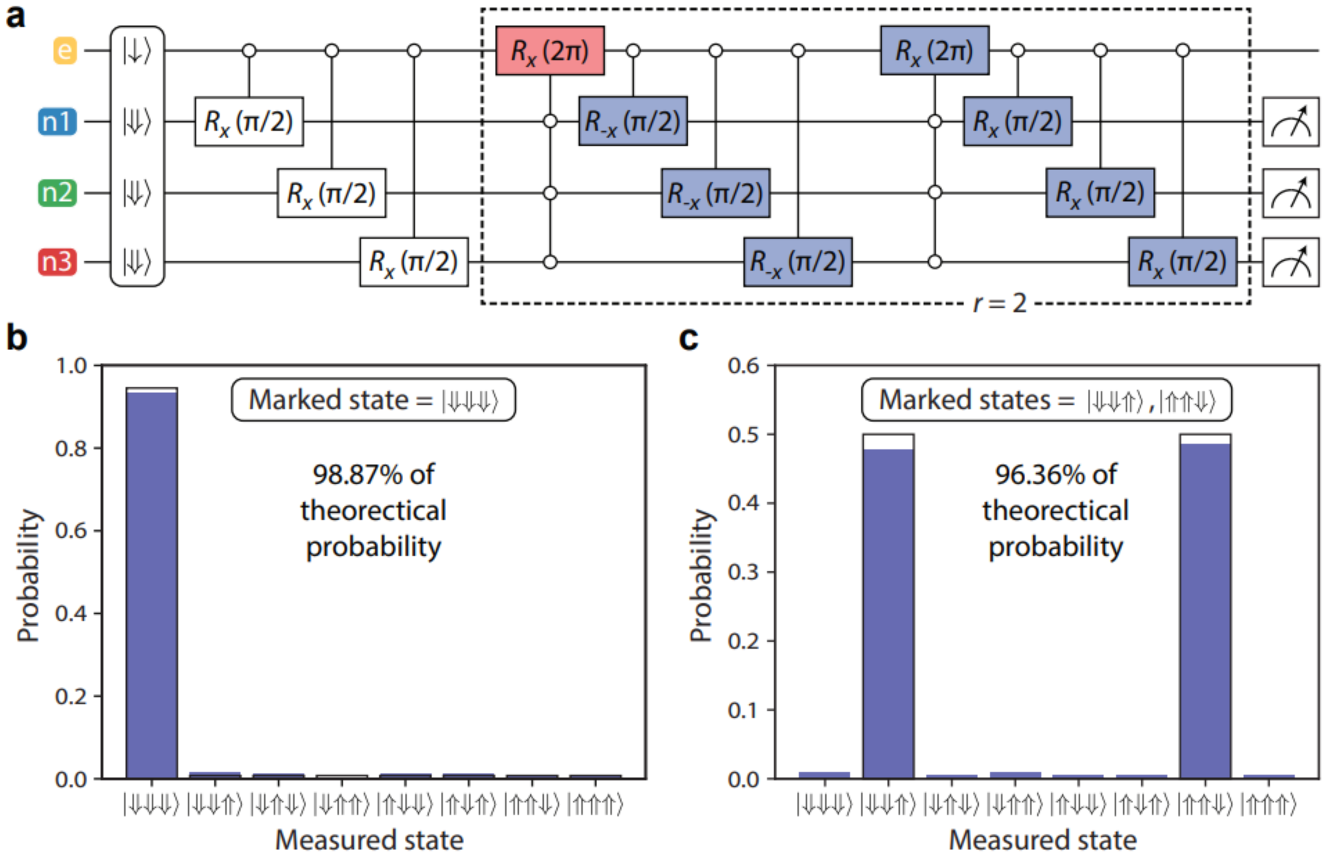
a
e
n1
n2
n3
|⇓⟩
R_x (π/2)
R_x (2π)
R_{-x} (π/2)
r = 2
b
Marked state = |⇓⇓⇓⟩
98.87% of theorectical probability
Probability
Measured state
c
Marked states = |⇓⇓⇑⟩, |⇑⇑⇓⟩
96.36% of theorectical probability
Probability
Measured state

www.acsnano.org

Machine Learning-Assisted Precision Manufacturing of Atom Qubits in Silicon

Aaron D. Tranter, Ludwik Kranz, Sam Sutherland, Joris G. Keizer, Samuel K. Gorman, Benjamin C. Buchler, and Michelle Y. Simmons*

Cite This: https://doi.org/10.1021/acsnano.4c00080

Read Online

ACCESS | Metrics & More | Article Recommendations | Supporting Information

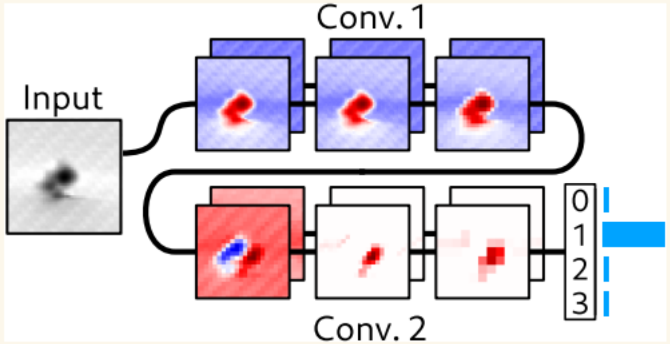

ABSTRACT: Donor-based qubits in silicon, manufactured using scanning tunneling microscope (STM) lithography, provide a promising route to realizing full-scale quantum computing architectures. This is due to the precision of donor placement, long coherence times, and scalability of the silicon material platform. The properties of multiatom quantum dot qubits, however, depend on the exact number and location of the donor atoms within the quantum dots. In this work, we develop machine learning techniques that allow accurate and real-time prediction of the donor number at the qubit site during STM patterning. Machine learning image recognition is used to determine the probability distribution of donor numbers at the qubit site directly from STM images during device manufacturing. Models in excess of 90% accuracy are found to be consistently achieved by mitigating overfitting through reduced model complexity, image preprocessing, data augmentation, and examination of the intermediate layers of the convolutional neural networks. The results presented in this paper constitute an important milestone in automating the manufacture of atom-based qubits for computation and sensing applications.

KEYWORDS: *machine learning, silicon, phosphorus, STM lithography, quantum dots*

Universität Basel

Single-qubit operations (e-qubit)

Nuclear spin state	f_{Rabi} (kHz)	T_2^* (μs)
$\lvert\Downarrow\Downarrow\Downarrow\rangle$	171.57	28.10
$\lvert\Downarrow\Downarrow\Uparrow\rangle$	170.67	31.43
$\lvert\Downarrow\Uparrow\Downarrow\rangle$	172.27	33.60
$\lvert\Downarrow\Uparrow\Uparrow\rangle$	172.01	30.79
$\lvert\Uparrow\Downarrow\Downarrow\rangle$	168.63	26.71
$\lvert\Uparrow\Downarrow\Uparrow\rangle$	171.04	38.26
$\lvert\Uparrow\Uparrow\Downarrow\rangle$	170.64	37.75
$\lvert\Uparrow\Uparrow\Uparrow\rangle$	171.29	26.73

Two and three qubit entanglement

$|\Downarrow\Downarrow\Downarrow\rangle$ state

Randomized benchmarking

$|\Downarrow\Downarrow\Downarrow\rangle$ state

Randomized benchmarking

A random Clifford gate $\sim$ 1.875 physical gate

$|\Downarrow\Downarrow\Downarrow\rangle$ state

Randomized benchmarking for a single qubit

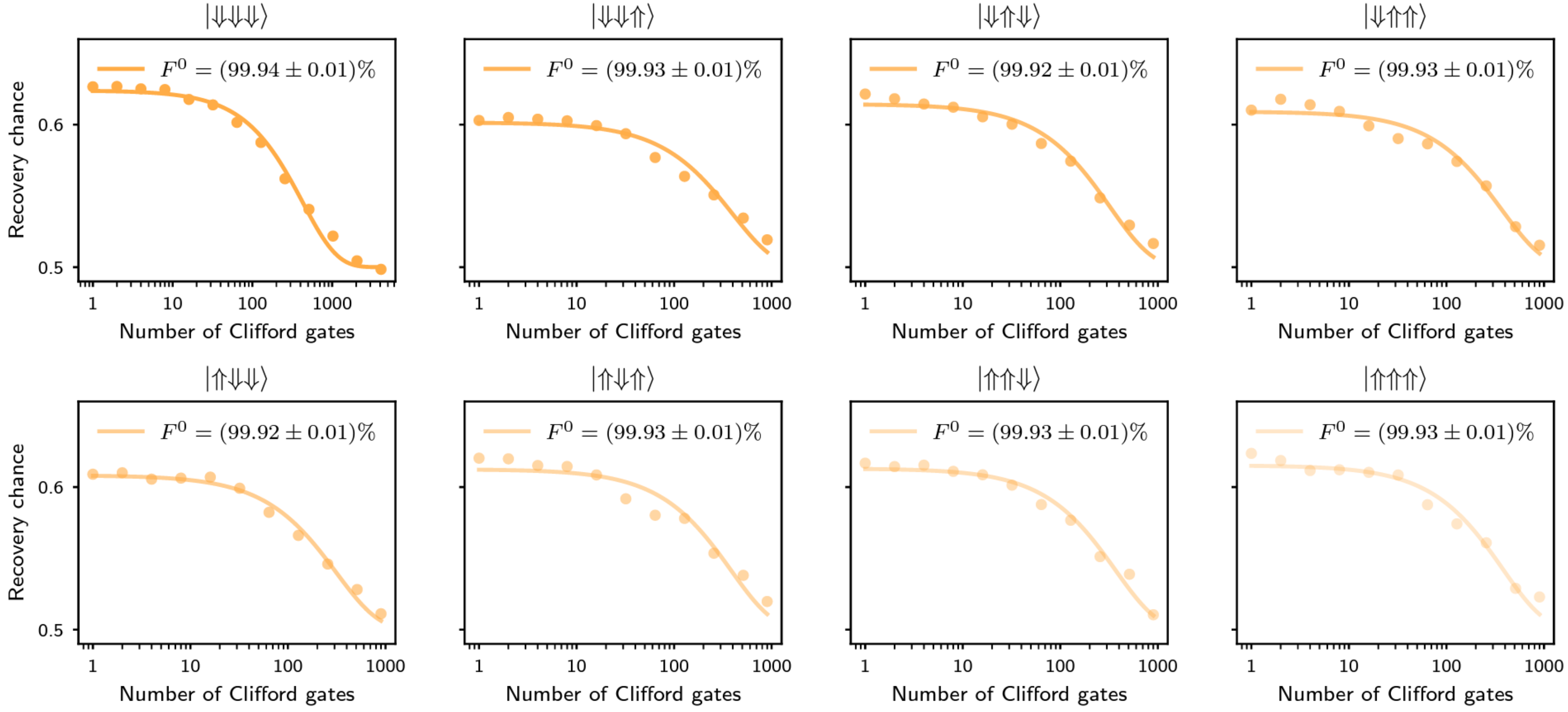

Bell's state tomography